

COMPRESSOR TANDEM BLADE AEROTHERMODYNAMIC
PERFORMANCE EVALUATION USING CFD

A THESIS SUBMITTED TO
THE GRADUATE SCHOOL OF NATURAL AND APPLIED SCIENCES
OF
MIDDLE EAST TECHNICAL UNIVERSITY

BY

ÇAĞRI GEZGÜÇ

IN PARTIAL FULFILLMENT OF THE REQUIREMENTS
FOR
THE DEGREE OF MASTER OF SCIENCE
IN
AEROSPACE ENGINEERING

SEPTEMBER 2012

Approval of the thesis:

**COMPRESSOR TANDEM BLADE AEROTHERMODYNAMIC
PERFORMANCE EVALUATION USING CFD**

submitted by **ÇAĞRI GEZGÜÇ** in partial fulfillment of the requirements for
the degree of **Master of Science in Aerospace Engineering Department,**
Middle East Technical University by,

Prof. Dr. Canan ÖZGEN
Dean, Graduate School of **Natural and Applied Sciences** _____

Prof. Dr. Ozan Tekinalp
Head of Department, **Aerospace Engineering** _____

Prof. Dr. İ. Sinan Akmandor
Supervisor, **Aerospace Engineering Dept., METU** _____

Assoc. Prof. Dr. Oğuz Uzol
Co-Supervisor, **Aerospace Engineering Dept., METU** _____

Examining Committee Members:

Prof. Dr. M. Cevdet Çelenligil
Aerospace Engineering Dept., METU _____

Prof. Dr. İ. Sinan Akmandor
Aerospace Engineering Dept., METU _____

Assoc. Prof. Dr. Oğuz Uzol
Aerospace Engineering Dept., METU _____

Assoc. Prof. Dr. D. Funda Kurtuluş
Aerospace Engineering Dept., METU _____

Asst. Prof. Dr. K. Melih Güleren
Aeronautical Engineering Dept., UTAA _____

Date: 07.09.2012

I hereby declare that all information in this document has been obtained and presented in accordance with academic rules and ethical conduct. I also declare that, as required by these rules and conduct, I have fully cited and referenced all material and results that are not original to this work.

Name, Last Name : Çaęrı GEZGÜÇ

Signature :

ABSTRACT

COMPRESSOR TANDEM BLADE AEROTHERMODYNAMIC PERFORMANCE EVALUATION USING CFD

GEZGÜÇ, Çağrı

M.Sc., Department of Aerospace Engineering

Supervisor: Prof. Dr. İbrahim Sinan AKMANDOR

Co-Supervisor: Assoc. Prof. Dr. Oğuz UZOL

September 2012, 56 pages

In this study, loss and loading characteristics of compressor tandem blades are evaluated. Whole study was focused on change of the total camber so called turning angle. Effects of camber change were investigated in terms of loss and loading characteristics. Methodology was increasing overall camber first by aligning angular positions of blades and second, if required, using more cambered airfoils.

2-dimensional cascade flow CFD analyses were performed to obtain loss-loading information of different tandem blade combinations. Acquired results were compared with the classical axial compressor blades' loading and loss characteristics which were obtained from literature. Results showed that most of the time tandem blade configuration performed better than the single blade counterpart in 2-dimensional cascade flow.

Lastly, to clarify the benefit of the study and present the gained performance in numbers, only one cascade flow CFD analysis was performed for a classical single compressor blade. Loss and loading results were compared with the tandem blade counterpart where single and tandem configurations both having the same degree of camber. It was clearly seen that tandem blade performed better again.

Keywords: turbomachinery, compressor, tandem blade

ÖZ

HAD KULLANARAK ÇİFT KOMPRESÖR KANADIN AEROTERMODİNAMİK PERFORMANS HESABI

GEZGÜÇ, Çağrı

Yüksek Lisans, Havacılık ve Uzay Mühendisliği Bölümü

Tez Yöneticisi: Prof. Dr. İbrahim Sinan AKMANDOR

Ortak Tez Yöneticisi: Doç. Dr. Oğuz UZOL

Eylül 2012, 56 sayfa

Bu çalışmada kompresörlerde çift kanatçık uygulamasının performansı değerlendirilmiştir. Çalışmada çift kanatçıklarda toplam kambur, yani akış dönüş açısı, değişiminin etkieri üzerine yoğunlaşmıştır. Bu etkiler kayıp ve yükleme özellikleri üzerinden değerlendirilmiştir. Çift kanatçığın toplam kamburunu artırmakta kullanılan yöntem; önce kanatçıkların açısız pozisyonlarının ayarlanması ve sonra, eğer gerekliyse, daha büyük kambura sahip kanatçık kullanılmasıdır.

Çift kanat kombinasyonlarının kayıp ve yükleme bilgilerini elde etmek amacıyla 2-boyutlu kaskad akışta HAD analizleri gerçekleştirilmiştir. Elde edilen sonuçlar, literatürde yer alan klasik tek kompresör kanadı kayıp ve yükleme verileri ile karşılaştırılmıştır. 2-boyutlu akış çözümlerinden elde edilen sonuçlarda, çift kompresör kanadının tek kompresör kanadına göre daha iyi sonuçlar verdiği gözlenmiştir.

Son olarak, yapılan çalışmanın faydasını açıkça ortaya koymak ve performans kazancını sayısal değerlerle göstermek amacıyla; sadece bir kez, klasik tek kompresör kanadı üzerinde kaskad akış için HAD analizi gerçekleştirilmiştir. Bu doğrultuda aynı kamber açlarına sahip çift kompresör kanadı ve eşleniği tek kompresör kanadı arasında kayıp ve yükleme değerleri kıyaslanmıştır. Çift kanadın daha iyi performans gösterdiği bu kıyaslamada da açıkça görülmüştür.

Anahtar Kelimeler: turbomakina, kompresör, çift kanatçık

*ođlu okusun diye altmıř yařına kadar dizinde ayakkabı dven Babaya;
okula a gitmesin diye gn ađarmadan uyanan Anaya;
bu can bin defa feda olsa, yine de yetmez...*

babama ve anneme...

ACKNOWLEDGEMENTS

I would like to express my utmost gratitude to my advisor, Prof. Dr. İbrahim Sinan Akmandor for providing academic guidance throughout my studies. I deeply appreciate his friendship and his patience to my philosophy of life as well. I am also grateful to my Co-Supervisor Assoc. Prof. Dr. Oğuz Uzol to his patience and assistance especially during the lecture period of the master's program.

I would like to thank to Roketsan for letting me use computer resources and licensed programs. Thanks to Uğur Arkun, who is the manager of my department at Roketsan, for his deep understanding and tolerance during the period of this M.Sc. program. And also I would like to thank to Bora Kalpaklı whom I have learned how to build up a Linux Computer Cluster that I had used during my thesis study.

I wish to acknowledge Erdem Ayan who has encouraged me while I was very hopeless for the studies going bad and tiring. I also wish to thank to Serhat Akgün for his help while pressing and distributing copies of this thesis.

Lastly, I express my deep gratitude to my brothers Ahmet, Ali, İsa and Yusuf, whom I shared more than 15 years of my 28-year old life, helped me so much during my university life.

TABLE OF CONTENTS

ABSTRACT.....	iv
ÖZ.....	vi
ACKNOWLEDGEMENTS.....	ix
TABLE OF CONTENTS.....	x
LIST OF TABLES.....	xii
LIST OF FIGURES.....	xiii
LIST OF SYMBOLS.....	xv
CHAPTERS	
1. INTRODUCTION.....	1
1.1 Background.....	2
1.2 Literature Review.....	4
1.3 Objectives.....	9
2. FLOW DOMAIN SET-UP.....	11
2.1 2-D Flow Domain Set-Up.....	11
2.1.1 Airfoil Data.....	11
2.1.2 In-House Code.....	11
2.1.3 Airfoils Placement.....	13
2.1.4 Creating Flow Domain.....	15
2.1.5 Mesh and Boundary Conditions.....	16
2.2 Tips and Tricks for Creating Flow Domain.....	20
3. SOLVER AND TEST MATRIX.....	22
3.1 Solver and Theory.....	22
3.1.1 Solver.....	22
3.1.2 Theory.....	23
3.2 Solution Techniques.....	25
3.2.1 Full Multigrid Solution.....	25
3.2.2 Changing Static Pressure.....	26
3.3 Test Matrix.....	26
4. RESULTS.....	28

4.1	2-Dimensional Results.....	30
4.1.1	NACA 65 506-606	34
4.1.2	NACA 65 506-906	37
4.1.3	NACA 65 506-1206	41
4.1.4	NACA 65 906-1206	42
4.2	Generalization of 2-Dimensional Results	45
5.	CONCLUSION	50
4.3	Main Results	50
4.4	Future work	51
	REFERENCES.....	52
	APPENDICES	
	APPENDIX A PRESSURE INLET vs. PRESSURE FAR FIELD BOUNDARY CONDITOINS.....	55

LIST OF TABLES

TABLES

Table 1 Geometric Variables [1]	4
Table 2 Experimental Set-Up Characteristics [4].....	5
Table 3 Controlled Variables [5].....	7
Table 4 3-D Rotor Characteristics [1,11]	8
Table 5 Mesh Independency Analyses Results	18
Table 6 Boundary Conditions for 2-D study	20
Table 7 2-D Tandem Airfoil Configurations.....	27
Table 8 Geometry and Performance Values of 506-606 Pair.....	35
Table 9 Geometry and Performance Values of 506-906 Pair.....	38
Table 10 Comparison of Single – Tandem Airfoil.....	40
Table 11 Geometry and Performance Values of 506-1206 Pair.....	41
Table 12 Geometry and Performance Values of 906-1206 Pair.....	43
Table 13 Comparison of Performance Values.....	55
Table 14 Comparison of Loading.....	55

LIST OF FIGURES

FIGURES

Figure 1 Flapped Airfoil [25]	1
Figure 2 Tandem Blades	2
Figure 3 Tandem Airfoil Terminology [1]	3
Figure 4 Tandem Rotor Set-Up [4]	5
Figure 5 Tandem Rotor Compressor [4]	6
Figure 6 Details of Set-Up [4]	6
Figure 7 Increasing Overall Camber	10
Figure 8 Flow Chart for Fortran Program	12
Figure 9 Original Airfoil	13
Figure 10 Rotated Forward Airfoil	13
Figure 11 Aft Airfoil Operations	14
Figure 12 Tandem Airfoil Geometry	14
Figure 13 Cascade (2-D) Flow Domain Geometry	15
Figure 14 Different Sized Meshes for Mesh Independency Study	17
Figure 15 2-D Mesh	18
Figure 16 Directions of Aerodynamic Forces	30
Figure 17 Sample Loss Bucket	31
Figure 18 Wall y^+ Distribution Over Airfoil Surfaces (NACA 65 906 - 1206 $K_{21}=50^\circ$ case)	32
Figure 19 Residuals (NACA 65 906 - 1206 $K_{21}=50^\circ$ case)	33
Figure 20 Convergence of Inlet Mach Number (NACA 65 906 - 1206 $K_{21}=50^\circ$ case)	33
Figure 21 Convergence of Inlet-Outlet Mass Flow Difference (NACA 65 906 - 1206 $K_{21}=50^\circ$ case)	34
Figure 22 NACA 65 506-606 Airfoil Pair With Inlet Blade Metal Angles	35
Figure 23 Loss Bucket of Separated Case ($K_{21}=40^\circ$)	36
Figure 24 Mach Contours of Separated Case ($K_{21}=40^\circ$)	36
Figure 25 Mach Distribution of $K_{21}=50^\circ$ Case	37

Figure 26 NACA 65 506 - 906 Airfoil Pair With Inlet Blade Metal Angles....	38
Figure 27 Mach Distribution of $K_{21}=60^\circ$ Case.....	39
Figure 28 Mach Contours of Single Airfoil (NACA 65-1006)	40
Figure 29 NACA 65 506-1206 Airfoil Pair With Inlet Blade Metal Angles....	41
Figure 30 Mach Distribution of $K_{21}=55^\circ$ Case.....	42
Figure 31 NACA 65 906 - 1206 Airfoil Pair With Inlet Blade Metal Angles..	43
Figure 32 Mach Distribution of $K_{21}=60^\circ$ Pair	44
Figure 33 Mach Contours of $K_{21}=50^\circ$ Case	45
Figure 34 Scatter of Tandem Airfoil Performance Values.....	46
Figure 35 Loss-Loading Trends of Different Tandem Airfoil.....	47
Figure 36 Change of D-factor by Overall Camber	48
Figure 37 Change of Loss Parameter by Overall Camber	48
Figure 38 Mach Contours of Pressure Inlet Case.....	56
Figure 39 Mach Contours of Pressure Far Field Case.....	56

LIST OF SYMBOLS

a	Speed of Sound [m/s]
AA	Aft Airfoil
AO	Axial Overlap
c	Chord
CFD	Computational Fluid Dynamics
D	Diffusion Factor
FA	Forward Airfoil
M	Mach Number
\dot{m}	Mass Flow Rate [kg/s]
P	Pressure [Pa]
PP	Percent Pitch
s	Spacing
T	Temperature [K]
t	Pitch Distance
U	Rotor Rotation Speed and Absolute Velocity [m/s]
W	Flow Velocity in Cascade Reference of Frame [m/s]

Greek Letters

α	Angle of Attack [degree]
β	Flow Angle [degree]
θ^*	Boundary Layer Momentum Thickness at Trailing Edge
K	Blade Metal Angle [degree]
σ	Solidity
Φ	Camber (degree)
ω	Loss

Subscripts:

1	Inlet
2	Exit

11	Forward Airfoil Inlet
12	Forward Airfoil Exit
21	Aft Airfoil Inlet
22	Aft Airfoil Exit
c	Coefficient
i	Tensor Indices
p	Parameter
t	Total of Quantity (Stagnation)
x	x-direction
y	y-direction
z	z-direction
θ	Tangential Direction

CHAPTER 1

INTRODUCTION

Tandem blade application in compressors has been worked since 1980's. Idea was using two blades in a row in axial direction with a small gap between them which is in tangential direction. This is the same as a flapped wing, where momentum transfer occurs from pressure side of the wing to the suction side at the flap region. Therefore, flapped wing can work under highly cambered conditions without losing lift generation capability. Same thing was applied to axial compressor blades while loading them to high levels. Highly cambered tandem blade configurations can be used for high loading. Although high degree of camber has the potential of separation, the gap between two blades reduces that risk over the aft blade. Moreover, velocity of fluid is increased while passing through this gap which leads to lowering the boundary layer momentum thickness over the aft blade. Furthermore, reduced boundary layer momentum thickness means lower loss, so better efficiency. As a result, tandem blade idea brings an efficient solution for highly loaded compressor blades.

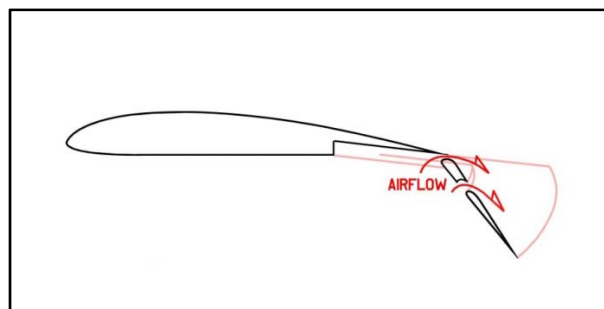


Figure 1 Flapped Airfoil [25]

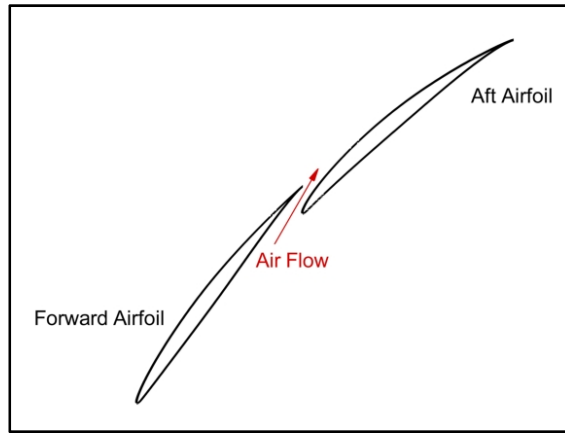


Figure 2 Tandem Blades

1.1 Background

Looking at the Euler Turbomachinery Equation [1.1] which obviously indicates there are two ways of achieving high loading at compressor blades. First one is increasing the rotational speed. Second one is increasing the tangential velocity difference between inlet and exit of a compressor rotor. That is increasing the turning angle.

$$\frac{-P_{\text{shaft}}}{\dot{m}} = (U_2 V_{\theta 2} - U_1 V_{\theta 1}) \quad [1.1]$$

In this study, rotational speed was not considered because all analyses were performed in cascade frame of reference. Remaining solution for high loading was increasing the turning angle, which is the tandem blade concept in this study, and has been better acquired during the literature survey. Most impressing study was a Ph.D. Thesis written by McGlumphy [1]. This work has a very deep research of literature on tandem airfoils, splitters and slotted airfoils. Although he explains other types of dual airfoils in his literature

survey, tandem blade and its application to an axial compressor rotor was the focus of that work. Thesis was based on numerical study. Both 2-D and 3-D CFD analyses were performed to see whether a tandem rotor is worth to apply on core part of an axial compressor or not. At the end, the answer was yes. This result gave the full motivation to this thesis work.

Figure 3 shows the variables related with the flow and tandem airfoil geometry. Furthermore, some equations relating those variables are listed in Table 1. Same notations with McGlumphy for tandem airfoil terminology have been used in this study. Because he had represented the things so methodically that everybody can understand easily [1].

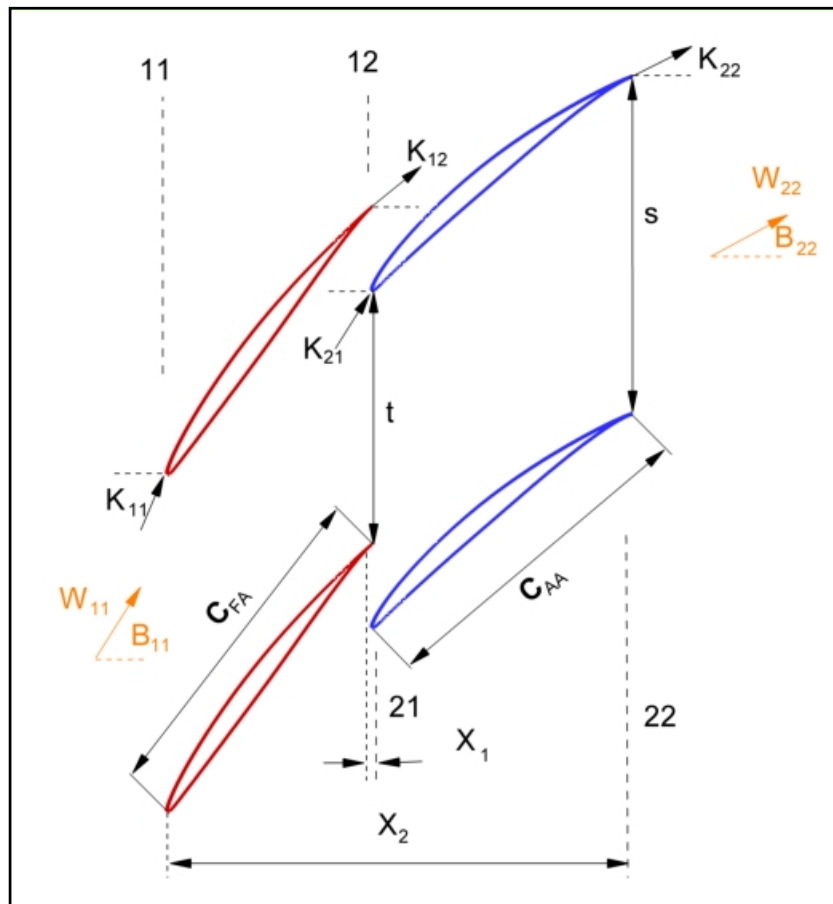


Figure 3 Tandem Airfoil Terminology [1]

Table 1 Geometric Variables [1]

Variable Name	Equation
Forward Airfoil Camber	$\phi_{FA} = K_{11} - K_{12}$
Aft Airfoil Camber	$\phi_{AA} = K_{21} - K_{22}$
Overall Camber	$\phi_{overall} = K_{11} - K_{22}$
Axial Overlap	$AO = X_1/X_2$
Effective Chord	$C_{eff} = (C_{FA} + C_{AA})/(1 + AO)$
Effective Spacing	$(1 - 0.5 * AO) * s$
Effective Solidity	$\sigma_{eff} = C_{eff}/s_{eff}$
Percent Pitch	$PP = t/s$

1.2 Literature Review

Looking at the history, tandem blade idea had been worked on for many times. Throughout these studies blade relative positions (in terms of angle and distance) and airfoil types are investigated. Some of the studies were performed to build tandem stators and some of them were to build tandem rotors. At the end, tandem stator applications are seen on commercial engines such as GE J79 [1], an advanced single-stage LP compressor designed by Honeywell [1] and GE MS 7001 EA heavy duty gas turbine [2]. However, tandem rotor concept has applications only for experimental purposes. Figure 4 indicates a photo of tandem rotor built at The Institute of Turbomachinery of The Hannover University.

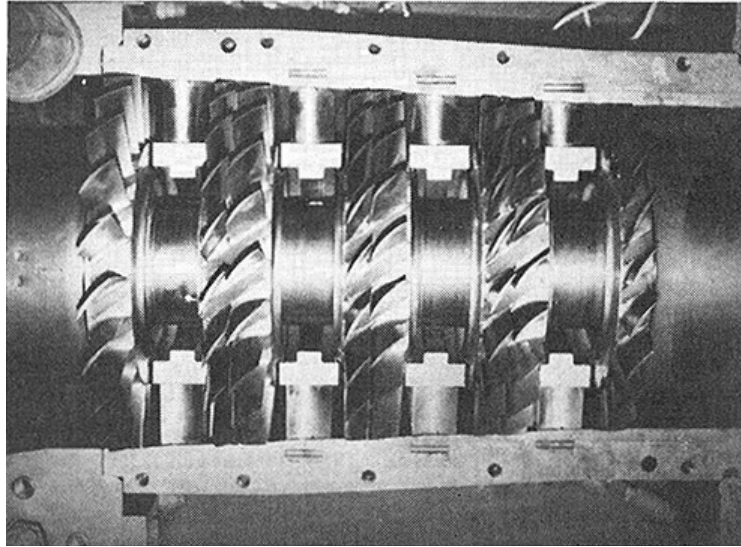


Figure 4 Tandem Rotor Set-Up [4]

One of the first tandem blade studies was performed in Germany [3-4]. This was a 4-stage axial compressor where 3 stages were built as tandem rotors and having a design pressure ratio of 2.5 [4]. Detailed characteristics of this experimental axial compressor are listed in Table 2.

Table 2 Experimental Set-Up Characteristics [4]

Name	Dimension	Value
Mass flow rate	kg / s	6.58
Speed	rpm	11000
Number of Stages	-	4
Design Pressure Ratio	-	2.50
Hub to Tip Ratio	-	0.64
Blade Tip Speed	m / s	195.82
Internal Power	kW	672
Inlet Total Pressure	bar	1
Inlet Total Temperature	K	288.15
Outlet Total Pressure	bar	2.51
Outlet Total Temperature	K	389.9

There are two papers explaining studies on this set up [3-4]. First one is an optimization study. Bammert & Staude spent effort on both theoretical and experimental jobs [3]. Theoretical calculations were performed by an

incompressible potential flow solver within an optimization study. For the experimental part it is stated that a four stage axial compressor was built. They had shown how tandem blades were optimized over the height for minimum profile losses and verification of their results with the experiments. Figure 5 illustrates a sketch of experimental set-up.

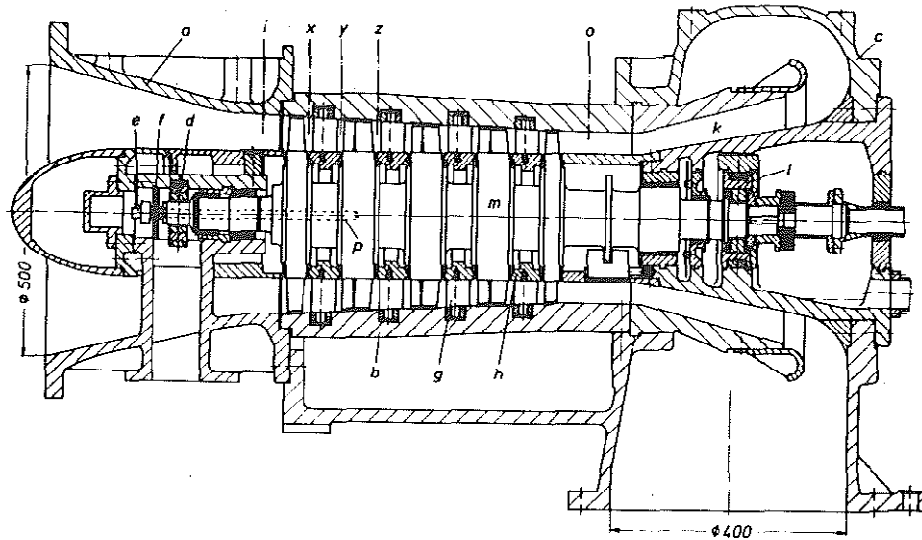


Figure 5 Tandem Rotor Compressor [4]

“(a) inlet casing, (b) stator blade carrier, (c) outlet casing, (d) journal bearing, (e) co-rotational transmitter, (f) receiving antenna, (g) stator blade, (h) shroud, (k) diffuser, (l) double thrust bearing, (m) rotor with rotor blades, (p) boring for transmitter line, (i, x, y, z, o) measuring plane for scanning” [4]

Details of stages and some geometrical information are presented in Figure 6.

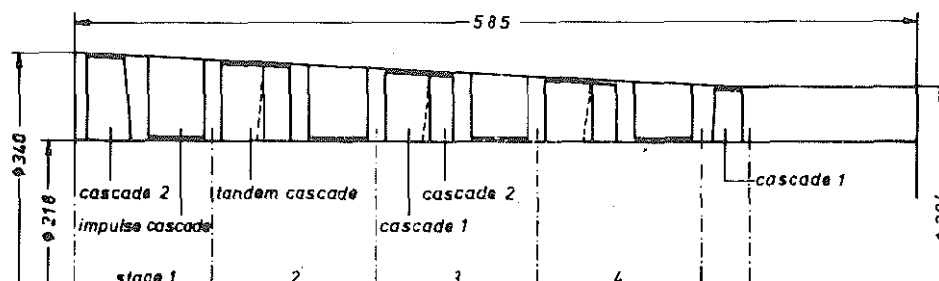


Figure 6 Details of Set-Up [4]

Further study on this set-up was conducted by Bammert & Beelte [4]. Experiments were performed at different rotational speeds so that they brought up compressor maps for five different stator combinations. They observed the effect of stagger angle change in stator blades. It is obviously seen that in the first paper they had tried to build up a compressor having optimized tandem rotor blades. Then in second paper, they had worked on stators to make it work better. Bringing these two results together, one can say that they got an axial compressor with optimized tandem rotor and improved stator blades. At the end, Bammert and Beelte clearly stated that tests had proven tandem rotor compressor did not raise any problems [4].

Another experimental work was performed by Nezym & Polupan [5]. Purpose of the study was obtaining a statistical-based correlation for the loss behavior of tandem cascade. During experiments six controlled variables, which were listed in Table 3, were investigated for minimum loss. Authors conclude that blade chord lengths, blade cambers and solidity should be taken into consideration when designing tandem cascades. Remaining variables did not have a dominant effect on tandem blade design.

Table 3 Controlled Variables [5]

No	Controlled Variable Definition
1	Axial overlap to forward airfoil's chord ratio
2	Displacement in peripheral direction to blade pitch ratio
3	Total chord to blade pitch ratio
4	Rear airfoil chord to forward airfoil chord ratio
5	Rear to forward airfoil camber ratio
6	Incidence

In addition to experimental effort, numerical studies on tandem blades were seen in literature. Those studies were pointing out consistent results with experiments. For instance, a 2-D study performed by McGlumphy was focusing on two parameters, which were percent pitch and axial overlap, in tandem arrangement of airfoils in cascade flow. He claimed that as percent pitch was increased up to a certain level, tandem airfoil performs better.

Moreover, axial overlap should be kept as zero to obtain the best performance and it is independent of airfoil combination [1,10]. In this thesis work, NACA 65 series airfoils were used as Bammert, Stadeu and Beelte did in their studies. It is due to the fact that NACA 65 series are widely used profiles in subsonic flow axial compressors. Moreover, there are lots of open information about this airfoil family in literature, some of them may be reached at references [6,12,16].

Further in his study, McGlumphy expresses results of his 3-D tandem rotor CFD analysis [1, 11]. Some geometrical information about this 3-D rotor is given in Table 4. Rotor was built for fully subsonic flows. It was a high hub to tip ratio rotor which was generated directly extruding from 2-D geometry into third dimension. Extruded geometry was selected from the prior study in his thesis work which has the best performance in 2-D CFD analyses. It is concluded that, results showed tandem rotor was worth to be used on an axial compressor.

Table 4 3-D Rotor Characteristics [1,11]

Name	Dimension	Value
Blade tip speed	m / s	212.75
Hub to Tip Ratio	-	>0.95
Effective Solidity	-	1.93
Axial Overlap	-	0.0
Percent Pitch	-	85%
Tip Clearance	mm	1.70
Overall Camber	deg	48.0

Furthermore, papers introducing the historical development of compressors light the author's way much. One of these papers was written by Wennerstrom and giving information of efficiently high loading of axial turbomachinery. It was stated that axial compressors have tendency for high efficiency while they have low aspect ratio blades [7,8]. Ball was also stating the same things in his paper [9]. He was indicating that designers first thought that high aspect ratio axial compressors were superior in terms of loading and efficiency. After a

while they saw that low aspect ratio designs had performed better. Therefore, tandem blade idea may be useful to build low aspect ratio compressor blades easily because of its inherently high effective chord length.

Besides the published information in literature, someone should look at the basics of axial compressor design while thinking of tandem blade idea. Entrance level theoretical information about turbomachinery and axial compressors may be gathered from text books [12-15].

Consequently, people have been working on tandem blades both in stators and rotors in axial machines for decades. Although some tandem stator applications have been seen in commercial engines, tandem rotor is still restricted to experimental compressors. On the other hand, there are CFD studies which showed tandem rotor performance ending with promising results.

1.3 Objectives

Main objective of the current work was evaluating the performance of tandem airfoils in 2-dimensional cascade flow using numerical tools. Simply effects of overall camber angle increment were interrogated. This is achieved in two different ways. First, an airfoil pair was selected and aft airfoil's inlet angle was decreased step by step. Therefore total camber of tandem airfoils reached higher values and this idea is indicated in Figure 7. Second method was obtaining a new tandem airfoil combination by just increasing backward or forward airfoil camber. That is using a more cambered airfoil directly.

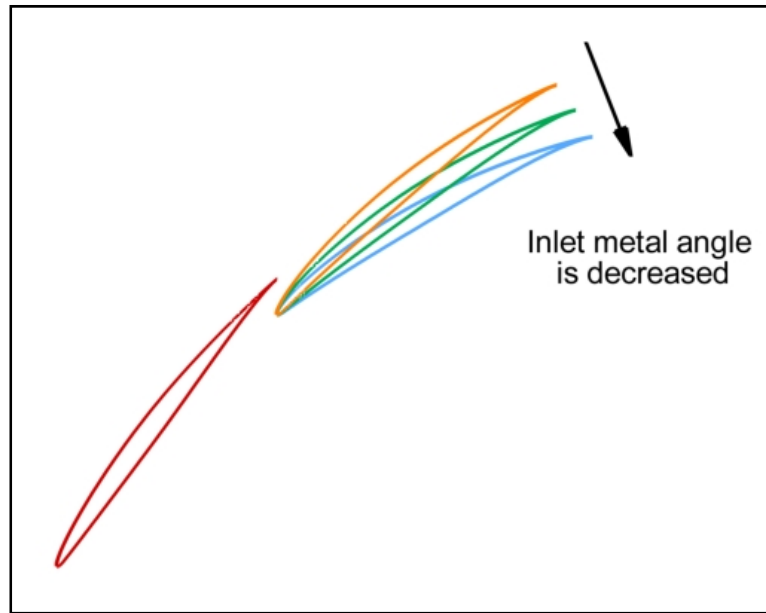


Figure 7 Increasing Overall Camber

CHAPTER 2

FLOW DOMAIN SET-UP

In this chapter basically four things will be handled. Section begins with the abilities of developed in-house code for 2-D flow domain creation. After that, mesh creation procedure is explained. At the end, whole analyses matrix is given and some tricks for preparing geometries to CFD analysis are shared.

2.1 2-D Flow Domain Set-Up

2.1.1 Airfoil Data

Airfoil data was generated from a Fortran code developed at NASA Glenn Research Centre. Program is able to generate NACA 4, 5 and 6 digit airfoils' data which is not only coordinates of points that are representing upper-lower surfaces and camber line of the airfoil but also first and second derivatives at each point. Moreover, it summarizes geometrical and aerodynamic characteristics of the airfoil. Detailed information can be obtained from reference [17].

2.1.2 In-House Code

An in-house Fortran code was written to get the numerical values of boundaries of a flow domain. This program is simply doing each and every repeated step for every tandem airfoil configuration automatically. That is, once the input file is given, this program aligns the airfoil positions, calls GAMBIT to draw and mesh the 2-D domain. After that calls the flow solver Fluent to start the CFD

solution. Finally, user takes the control in hand due to the CFD solution technique in turbomachinery problems which is expressed in Chapter 3. A flow chart is indicated in Figure 8 to visualize the procedure

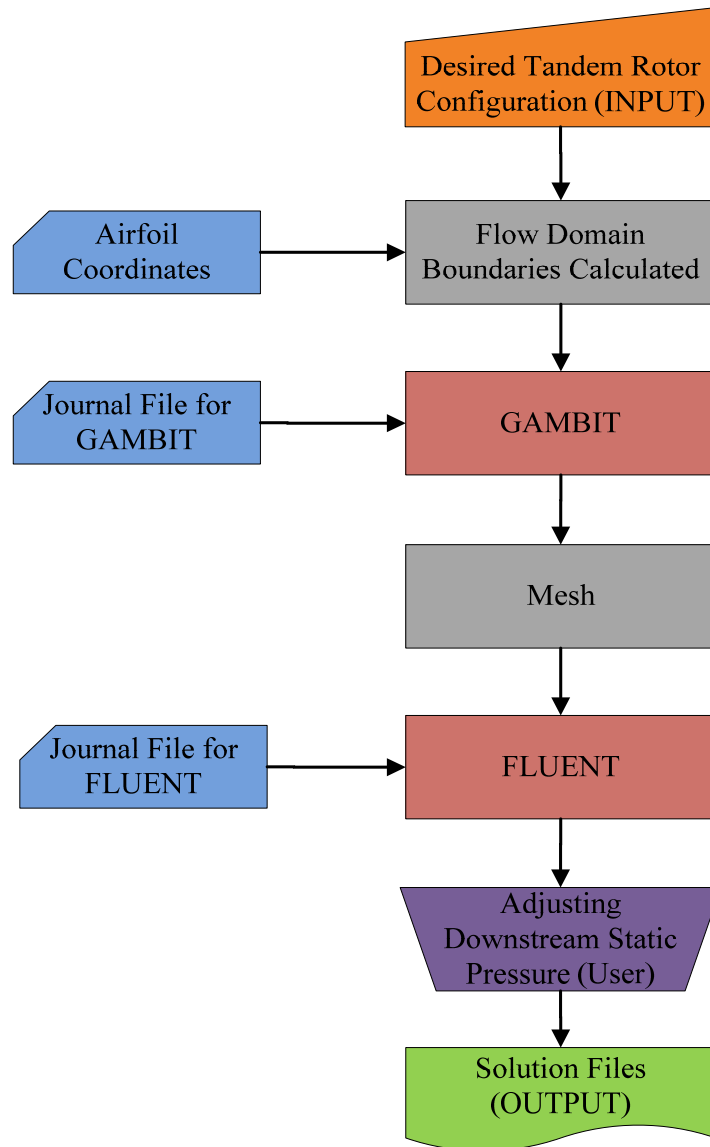


Figure 8 Flow Chart for Fortran Program

2.1.3 Airfoils Placement

For a 2-D flow domain, starting step is arranging airfoils and basically two things done. Firstly, airfoils are rotated about its quarter chord and adjusted to desired blade metal angle as indicated in Figure 9 and Figure 10.

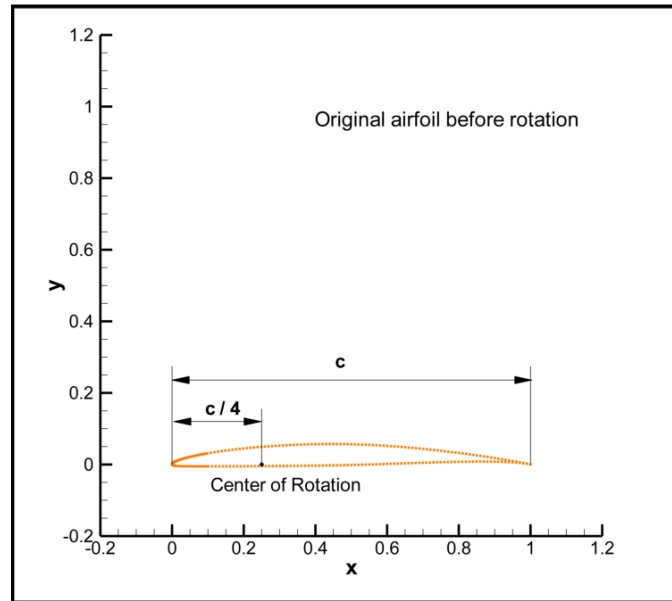


Figure 9 Original Airfoil

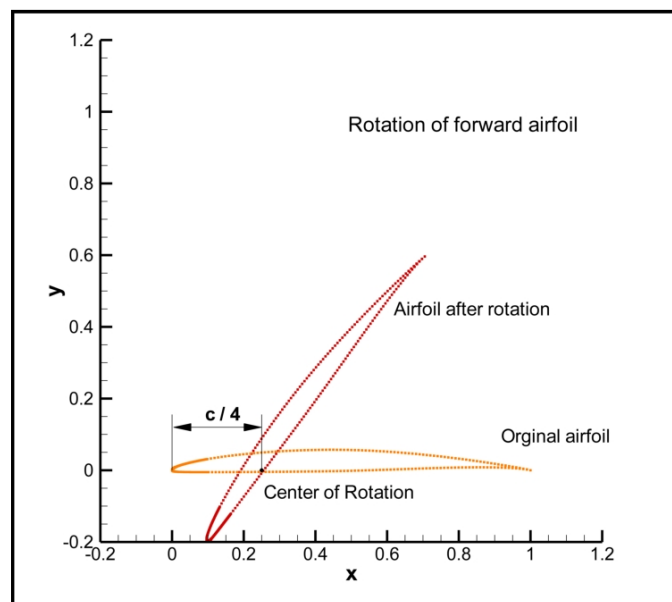


Figure 10 Rotated Forward Airfoil

Secondly, translation is performed for only the second airfoil. In fact, desired axial overlap and percent pitch values are reached by this way. Figure 11 and Figure 12 indicate respectively the translation operation and final tandem airfoil geometry.

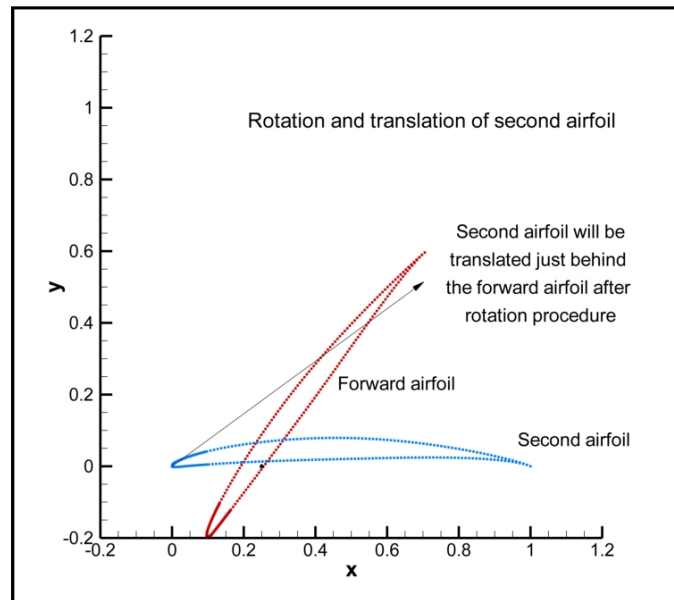


Figure 11 Aft Airfoil Operations

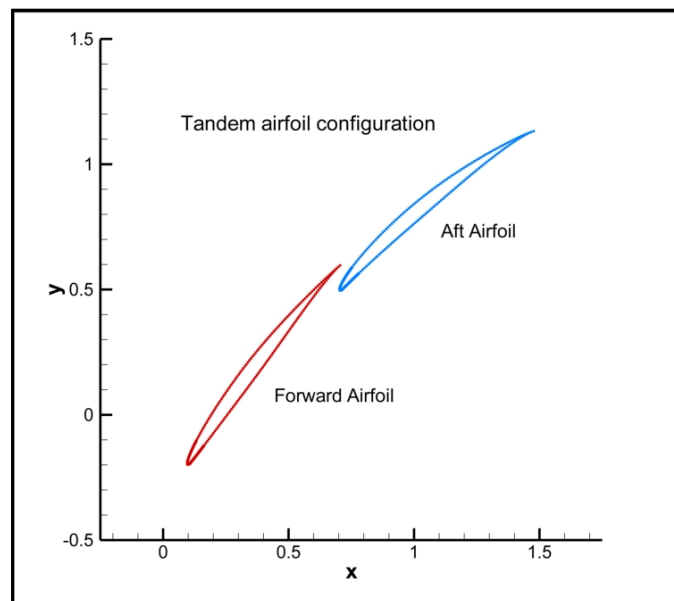


Figure 12 Tandem Airfoil Geometry

All geometries have zero axial overlap and 0.95 percent pitch value due to the fact that in his study McGlumphy has shown tandem blade performance is the best [1].

2.1.4 Creating Flow Domain

Flow domain is created in GAMBIT which is a commercial program. A journal file was prepared to build up the whole geometry in GAMBIT automatically. Basically in-house code sends a text file including coordinates of boundary points and airfoil data to GAMBIT. Then, GAMBIT processes this information as coded in the journal file.

While creating the geometry, upstream flow boundary was placed at 2.5 chord distance in front of the forward airfoil's leading edge and downstream side boundary was placed at 2 chord distance behind aft airfoil's trailing edge. These distances were decided after some trial solutions in CFD. The goal of those trails was to minimize the interaction of solution with boundaries. Figure 13 shows example flow domain geometry.

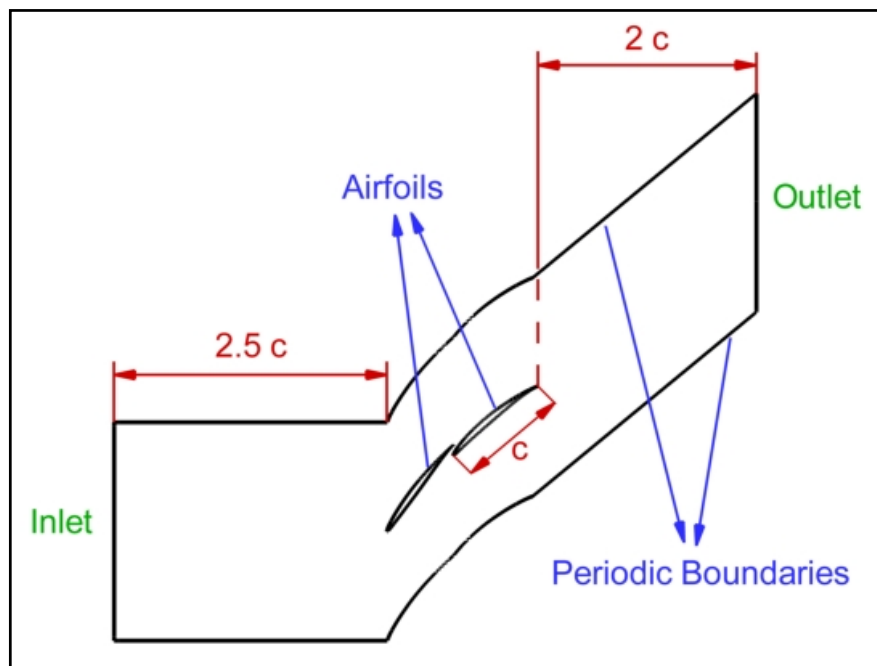


Figure 13 Cascade (2-D) Flow Domain Geometry

It is seen in Figure 13 that downstream part of the domain is not parallel to upstream part, but inclined with the same angle of aft airfoil's chord line. This is due not to interact wake region with periodic boundaries. As a result, ease of convergence is improved. Examples of similar flow domains can be seen at references [26,27].

2.1.5 Mesh and Boundary Conditions

GAMBIT has three different types of 2-D mesh options. These are quad (quadrilateral), tri (triangular) and quad-tri meshes. Due to the fact that it is easier to get a high quality mesh, unstructured triangular mesh option was used throughout this study.

A boundary layer was attached on airfoils. The criterion for boundary layer thickness was having a wall y^+ value less than 1. This is because of the turbulence model used by the solver. A useful tool for predicting boundary layer mesh thickness can be reached at reference [28] for a desired wall y^+ value.

After giving a decision to mesh type and boundary layer thickness, mesh independency analyses were performed. Four different size of mesh were studied for independency and presented in Figure 14.

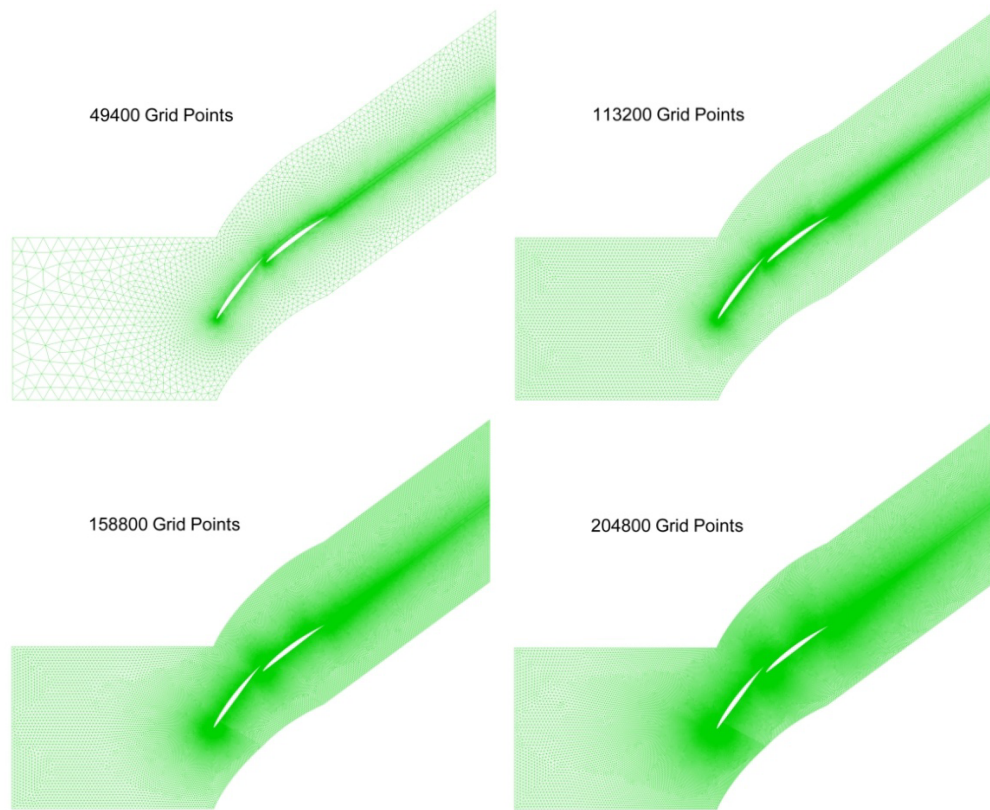


Figure 14 Different Sized Meshes for Mesh Independency Study

In reference [1] it is asserted that change of quantities less than 2% between two different sized meshes was enough for mesh independency. In this study, mesh sizes were adjusted as 2, 3 and 4 times of the coarsest mesh size as illustrated in Figure 14. Performance parameters were used as a measure of change in quantities. This is because; they are not obtained directly from CFD results but after some mathematical operations. Those mathematical operations make their error band become larger. Therefore, if they are within the desired range of change for mesh independency, then other quantities, which are directly obtained from CFD solution, such as temperature, pressure, velocities etc. are already in this desired range.

Table 5 Mesh Independency Analyses Results

<u>Number of Grid Points</u> 1000	% D-factor Change	% Loss Parameter Change	% Loss Coefficient Change
49.4 – 113.2	0.16	3.43	3.22
113.2 – 158.8	0.06	1.86	1.19
158.8 – 204.8	0.03	0.33	1.10

Table 5 shows the mesh size and change of performance values. Each row indicates the percent change of performance parameters between two different sized meshes. It is obviously seen that percent change of quantities between 113200 and 158800 grid point meshes are less than 2 which means 158800 grid points are enough to say mesh is independent from solution. Further analysis performed for double checking of the study. Solution of a 204800 grid point mesh was compared with the 158800 grid point mesh. Results of this analysis showed that change in performance quantities were even lower.

Consequently, mesh independency analyses were result in a domain of nearly 160.000 grid points and Figure 15 shows a meshed flow domain with a boundary layer detail.

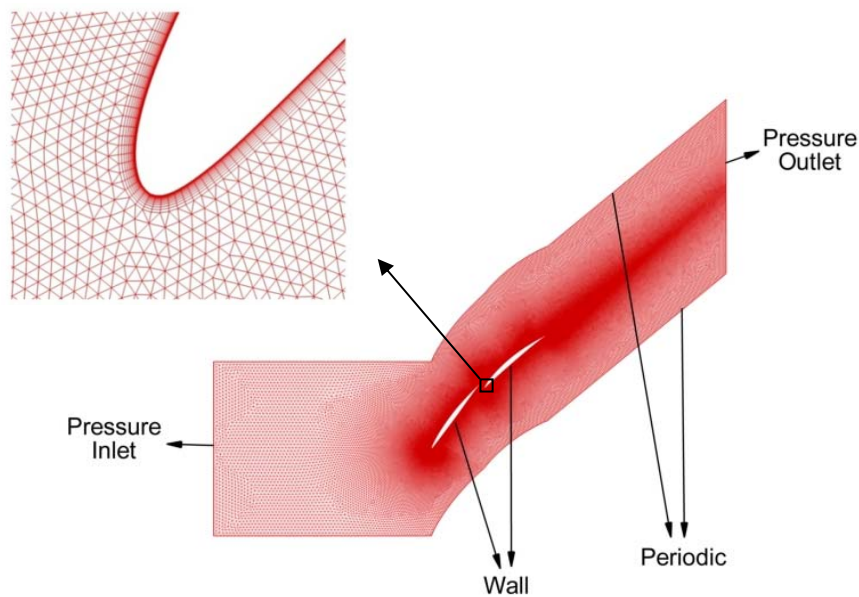


Figure 15 2-D Mesh

Up to here geometry and mesh generation of 2-D study is explained. Next step is boundary conditions. 2-D CFD study was performed for cascade flow solutions. Flow around the blades was desired to be shock free that is fully subsonic. As a result, it was decided to have a flow Mach number of 0.6 M at cascade inlet. There are two alternative boundary conditions to obtain 0.6 M at the inlet in Fluent. These are pressure inlet, which is widely used in turbomachinery applications, and pressure far field boundary conditions. First one lets the user to enter total pressure and temperature as a boundary condition, whereas second one needs static pressure with a target Mach number and the total temperature. During cascade flow study pressure inlet was preferred as upstream boundary condition. On the other hand, in Appendix A results for both upstream boundary conditions are compared. It was showed that results are close enough to use one of the alternative boundary conditions safely for cascade flow analyses.

For downstream boundary condition pressure outlet option was used. User need to define the static pressure at the exit and a back flow total temperature. If backflow occurs during the analysis, then this temperature information contributes for convergence. Otherwise temperature information is not used.

One more boundary condition is applied for viscous flow at upstream boundary. Turbulence quantities were defined uniformly as turbulence intensity and hydraulic diameter. These two turbulence quantity can be used safely for fully developed flows [18]. For downstream boundary, backflow turbulence quantities may be defined as well. However, these contributes to convergence if backflow occurs at the exit, otherwise all turbulence information is extrapolated from upstream [18].

The last boundary condition was applied for the periodicity. Passage boundaries were appointed as periodic.

Table 6 represents up and downstream flow boundary conditions.

Table 6 Boundary Conditions for 2-D study

Boundary	Name	Value
Operating Condition	Gauge Pressure	101325 Pa
Pressure Inlet	Total Pressure	27915 Pa
	Total Temperature	300 K
	Turbulence Intensity	0.03
	Hydraulic Diameter	0.03 m
Pressure outlet	Static Pressure	Changed
	Back Flow Total Temperature	300 K
	Turbulence Intensity	0.03
	Hydraulic Diameter	0.03 m
Wall	Stationary	-
Periodic	Translational	-

2.2 Tips and Tricks for Creating Flow Domain

In this part, some suggestions for solution of problems that were faced during the thesis work were given. These problems were related with automation of flow field creation, geometry and mesh generation.

First is about automation so the journal file. There are two ways of creating journal files. One way is building up geometry and mesh manually for the first time so that each and every step is recorded in a journal file by GAMBIT simultaneously. Then use that journal file for automated analyses. One has to be careful about ensuring that every step has been recorded correctly throughout the journal. In such a journal file somebody may change the numerical values which adjust distances or mesh size. On the other hand, do not try to change or delete any geometrical definition, because the result will probably be a total failure. Second way is defining variables first and then coding the flow domain directly in a journal file without visualization. After generating this data, run that journal file in GAMBIT to see the results. If something is wrong, the journal file has to be corrected accordingly. This is little bit time consuming but a much more robust method than the first way. Some explanations and examples may be obtained from references [2,19].

Second suggestion is about creating boundary layer. If GAMBIT is to be used as a mesher, one should be able to use Tgrid as well. Tgrid is absolutely superior on creating boundary layer and improved quality of mesh than GAMBIT. Although this thesis work is a 2-Ddimensional study, one should know that for 3-dimensional turbomachinery CFD applications GAMBIT is not able to produce a smooth geometry and a high quality boundary layer. However, Tgrid can do high quality job for such applications.

CHAPTER 3

SOLVER AND TEST MATRIX

This chapter divided into three main parts. It begins with a very brief introduction for the solver and theoretical bases. After that, solution techniques are summarized and some tricks are suggested. At the end, test matrix is given indicating which geometrical configurations of tandem airfoil analyses were performed in this thesis work.

3.1 Solver and Theory

3.1.1 Solver

This study was realized by the commercial CFD solver Fluent. Cascade flow problems were solved for compressible and viscous flow.

First of all, flow simulations were performed at high speeds. Flow Mach number at the cascade inlet was 0.6 M. If 0.3 M is considered to be the limit of incompressible flow, simulations must be performed obviously under compressible flow conditions. A second order pressure based solver was preferred during analyses. This pressure based solver was using pressure-velocity coupling method. It was observed that coupled solver in Fluent increases time for one iteration, yet decreases number of iterations very much during the convergence of solution. Therefore, it is logical to use the “coupled” solver in Fluent rather than “simple” solver in such a cascade simulation.

Secondly, it is claimed that tandem blade flow separation characteristics is better than classical blades [1]. Thus somebody must deal with boundary layer around blades so the viscous flow. As all other commercial CFD programs Fluent has its own turbulence models; starting from one equation Spalart-Allmaras to Large Eddy Simulation there are six of them. In this study, Spalart-Allmaras turbulence model had been used because it is widely used in turbomachinery applications and efficient in terms of computer resources [18]. Moreover, it is recommended that boundary layer mesh must be so fine near the wall surface that wall y^+ value should be kept under 1. As a result, a good solution can be obtained for turbulence modeling [18].

Consequently, working with high speed air flow in a turbomachinery application brought the necessity of dealing with compressible and viscous flow. A second order discretization was preferred for accuracy of solution and a one-equation model was thought to be enough for turbulence modeling.

3.1.2 Theory

Computational fluid dynamics is just solving fluid equations using numerical methods. Fluid equations are formed by conservation of quantities which are mass, momentum and energy. Moreover, some additional equations are used to solve compressibility and turbulence phenomena such as equation of state and modeled transport equations.

First equation is conservation of mass. It is a scalar quantity, so just one equation is enough to show that mass is conserved. Fluent solve the conservation of mass equation as in Equation [3.1].

$$\frac{\partial \rho}{\partial t} + \nabla \cdot (\rho \vec{v}) = S_m \quad [3.1]$$

“On the right hand side S_m is the mass added to the continuous phase from the dispersed second phase (e.g., due to vaporization of liquid droplets) and any user-defined sources” [18].

Second conservation equation belongs to linear momentum. Due to the fact that momentum is a vector quantity, somebody needs to write one equation for each dimension of the fluid problem. A 3-dimensional problem has 3 momentum conservation equations in x, y and z directions. In Fluent, momentum equation is represented as in Equation [3.2].

$$\frac{\partial}{\partial t}(\rho\vec{v}) + \nabla \cdot (\rho\vec{v}\vec{v}) = -\nabla p + \nabla \cdot (\bar{\tau}) + \rho\vec{g} + \vec{F} \quad [3.2]$$

“Where p is the static pressure, $\bar{\tau}$ is the stress tensor, and $\rho\vec{g}$ and \vec{F} are the gravitational body force and external body forces, respectively” [18].

While modeling 2-D cascade problems x and y momentum equations are enough to solve.

The last conservation equation comes from the energy. It is a scalar just as the mass. Therefore, only one equation is enough to represent energy conservation. Equation [3.3] is solved by Fluent for energy conservation.

$$\frac{\partial}{\partial t}(\rho E) + \nabla \cdot (\vec{v}(\rho E + p)) = \nabla \cdot (k_{\text{eff}}\nabla T - \sum_j h_j \vec{J}_j + (\bar{\tau}_{\text{eff}} \cdot \vec{v})) + S_h \quad [3.3]$$

“Where k_{eff} is the effective conductivity ($k+k_t$, where k_t is the turbulent thermal conductivity, defined according to the turbulence model being used), and \vec{J}_j is the diffusion flux of species j . The first three terms on the right-hand side of the energy equation represent energy transfer due to conduction, species diffusion, and viscous dissipation, respectively. S_h includes the heat of

chemical reaction and any other volumetric heat sources you have defined” [18].

In theory, all equations have their unknown term and can be listed as:

Conservation of mass and momentum	→	ρ, U_i, P
Conservation of Energy	→	T

For mass and momentum equations there are 5 unknowns for 4 equations in a 3-D problem. One more equation is needed to solve for the unknowns. Therefore, conservation of energy equation [3.3] is written as the fifth equation but it brings an unknown term as well. At the end, another equation is written which is the equation of state [3.4] to reach the number of equations to 6. Moreover, it doesn't have a new unknown term. Thus, totally there are 6 unknowns with 6 equations in hand which means it is mathematically possible to solve the problem.

$$P = \rho RT \quad [3.4]$$

If flow was incompressible then there was no need of energy [3.3] and state [3.4] equations. Because density is constant for incompressible flows, one mass conservation and three momentum equations will be enough to solve for 4 unknown terms which are pressure and three velocity components for a 3-dimensional problem.

3.2 Solution Techniques

3.2.1 Full Multigrid Solution

Full multigrid solution is a fast way of obtaining a simple solution for a CFD problem in Fluent. If full multigrid solution is not used; first, solver spends much more time and computational effort to get a meaningful flow path. Then

goes deeper in solution and converges to higher orders. Therefore, this simple solution contributes to solution by a good starting point.

3.2.2 Changing Static Pressure

In turbomachinery, classical boundary condition application is defining total quantities at the inlet and static pressure at the exit. Moreover, changing static pressure at the downstream boundary (exit) during an analysis, leads CFD users to adjust upstream (inlet) Mach number [20]. This method is used for design point CFD analysis. If somebody wants to perform off design analyses then need to define some mass flow rate information [21-23].

3.3 Test Matrix

In this part 2-D cascade flow test matrix is presented which is briefly giving information about tandem airfoil geometries. Besides that, it explains how controlled variables were decided and interrogated.

There are 8 different parameters which can be used while creating tandem airfoil geometry. Those variables were presented in Table 1. Among these parameters, airfoil cambers and difference between those two airfoils' blade metal angles ($K_{11} - K_{21}$) were selected. These three controlled variables were used to increase total camber of tandem airfoils. Other parameters all kept constant. According to McGlumphy, percent pitch should be as high possible (he worked up to 95% percent pitch value) and axial overlap must be 0 for the best performance [1]. Therefore, those two variables were set to 0.95 for percent pitch and 0 for axial overlap. Moreover, solidity and chord length were kept constant. During this study effective chord length for each airfoil was 34 mm and effective solidity was 1 for all geometries. There was no rounding at the leading or trailing edge of both airfoils as well. Table 7 indicates analyses matrix.

Table 7 2-D Tandem Airfoil Configurations

Tandem Airfoil	K_{11}	K_{21}	Φ_{FA}	Φ_{AA}	K_{22}	$\Phi_{overall}$
506-606	65.00	55.00	24.92	29.70	25.30	39.70
506-606	65.00	50.00	24.92	29.70	20.30	44.70
506-606	65.00	40.00	24.92	29.70	10.30	54.70
506-906	65.00	60.00	24.92	43.37	16.63	48.37
506-906	65.00	55.00	24.92	43.37	11.63	53.37
506-906	65.00	50.00	24.92	43.37	6.63	58.37
506-1206	65.00	60.00	24.92	55.87	4.13	60.87
506-1206	65.00	55.00	24.92	55.87	-0.87	65.87
906-1206	65.00	60.00	43.37	55.87	4.13	60.87
906-1206	65.00	55.00	43.37	55.87	-0.87	65.87
906-1206	65.00	50.00	43.37	55.87	-5.87	70.87

In Table 7, first column represents the airfoil names. All airfoils belong to NACA 65 series with a maximum thickness to chord ratio of 6%. As seen from the table overall camber was tried to increase both by increasing directly camber of airfoils and increasing the difference between forward and aft airfoils' blade metal angle ($K_{11} - K_{21}$). At the end, a test matrix was obtained with a camber range between 40° to 71°.

CHAPTER 4

RESULTS

This section reviews the results of CFD analyses. Performance parameters, normalized lift distribution and Mach contours of CFD results were represented.

Performance parameters are divided into two. D-factor is a representation of loading; loss coefficient and loss parameter are indicators of losses.

Loading was determined by D-factor which was defined by Lieblein first [6]. It is a diffusion parameter independent of blade shapes where velocity distribution data are not available. Equation [4.1] indicates the Lieblein definition of D-factor.

$$D = \left(1 - \frac{W_2}{W_1}\right) + \left(\frac{\Delta W_\theta}{2\sigma W_1}\right) \quad [4.1]$$

In his study McGlumphy defines D-factor for a tandem blade as Equation [4.2]. Same definition was used throughout this thesis as well.

$$D = \left(1 - \frac{W_{22}}{W_{11}}\right) + \left(\frac{W_{\theta,11} - W_{\theta,22}}{2\sigma_{\text{eff}} W_{11}}\right) \quad [4.2]$$

Loss coefficient is used as a measure of total pressure loss across the blades. It is defined in Equation [4.3] as total pressure change normalized by inlet dynamic pressure.

$$\omega_c \equiv \frac{P_{t,11} - P_{t,22}}{P_{t,11} - P_{11}} \quad [4.3]$$

Loss parameter indicates the non-dimensional boundary layer momentum thickness. Equation [4.4] represents loss parameter.

$$\omega_p \equiv \left(\frac{\theta^*}{C_{eff}} \right) \quad [4.4]$$

For tandem blade loss parameter is adapted by McGlumphy in reference [1]. It is shown in Equation [4.5] and same definition is used in this study as well.

$$\omega_p \approx \omega_c \frac{\cos\beta_{22}}{2\sigma_{eff}} \left(\frac{\cos\beta_{22}}{\cos\beta_{11}} \right)^2 \quad [4.5]$$

Lift distribution between forward and aft airfoils was observed during analyses as well. In theory, aerodynamic lift is defined as the force over a wing which is in the normal direction to free stream flow. In tandem airfoil case there is no problem with the forward airfoil while calculating lift. However, for the aft airfoil free stream velocity may be discussed. Due to the fact that forward airfoil is disturbing the flow, free stream angle will change before flow reaches the aft airfoil's leading edge. It is hard to determine the right free stream angle before second airfoil. Thus, free stream angle for aft airfoil was assumed to be the same with the forward airfoil. Then lift calculations were realized. Figure 16 indicates aerodynamic forces on both airfoils.

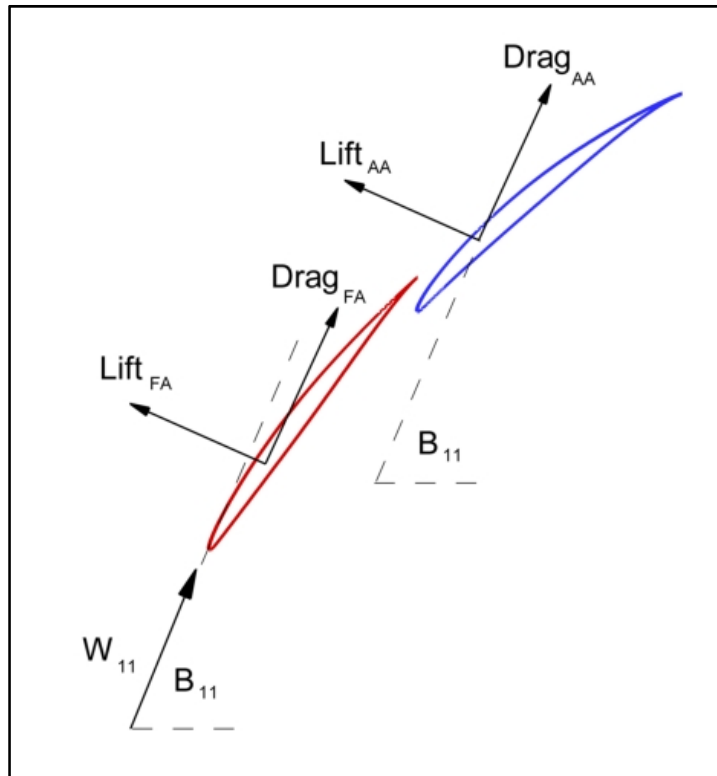


Figure 16 Directions of Aerodynamic Forces

4.1 2-Dimensional Results

In this part, result of cascade study is reviewed. Cascade analyses were performed for different inlet flow angles to determine the corresponding loss coefficient. Therefore, minimum loss coefficient would bring the on design (design point) information for that geometry. Technically speaking, cascade study was based on a partial loss bucket analysis. Aim of this thesis work was not obtaining the full loss bucket, so the off-design information for a tandem airfoil geometry. Purpose was just to evaluate design point performance. In spite of the fact that Figure 17 shows a full loss bucket of only one tandem airfoil configuration, analyses for other geometries were performed up to a certain point that minimum loss was assured to be reached.

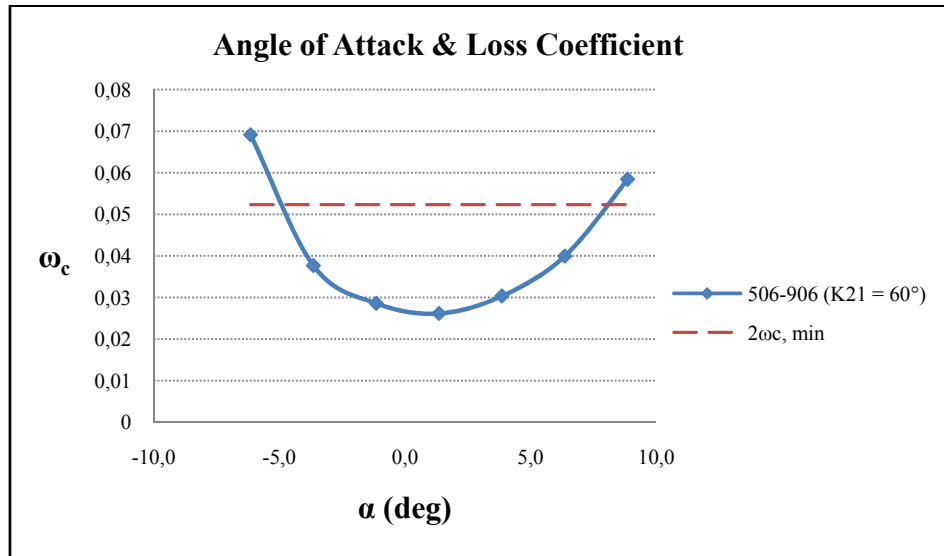


Figure 17 Sample Loss Bucket

Following subtitles devoted to results of design point analyses, which were presented as tables, graphs and contours for each geometry. Basically D-factor, loss coefficient, loss parameter and lift of airfoils are observed. In these tables “normalized loading” means that aft or forward airfoil’s lift normalized by that tandem airfoil’s total lift. In fact, it is the lift distribution on both airfoils.

As mentioned in Chapter 3, wall y^+ values for all analyses were kept below 1 for the health of turbulence modeling of Spalart – Allmaras. Figure 18 indicates an example wall y^+ distribution on both airfoils (NACA 65 906 - 1206 $K_{21}=50^\circ$ case).

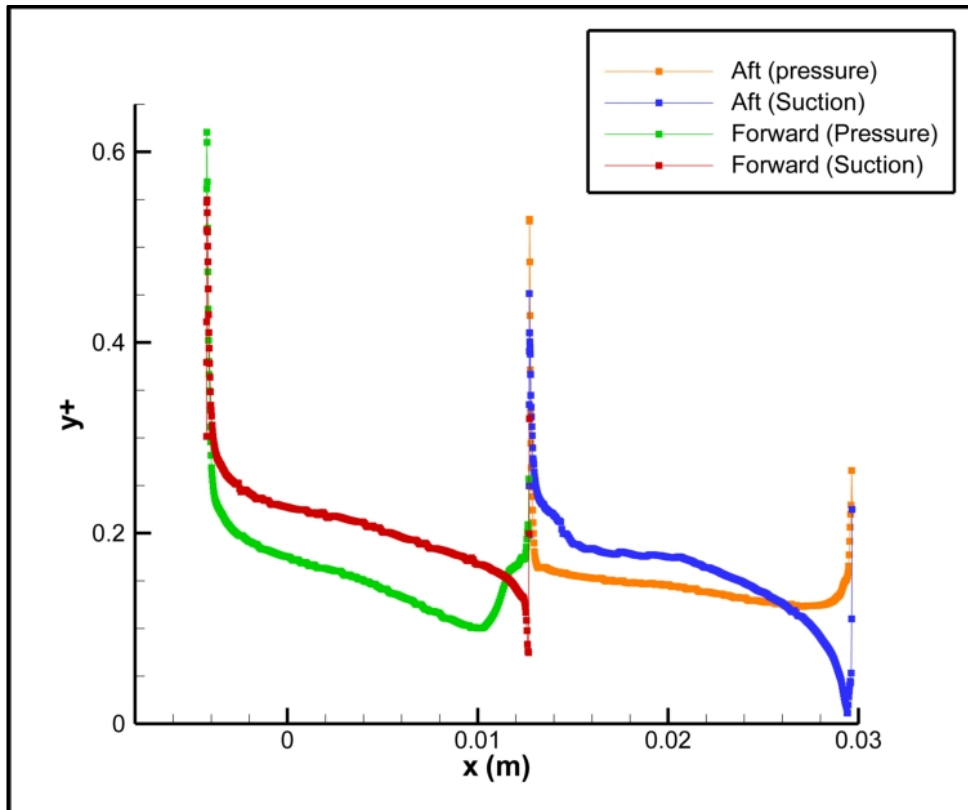


Figure 18 Wall y^+ Distribution Over Airfoil Surfaces (NACA 65 906 - 1206 $K_{21}=50^\circ$ case)

Further information about analyses is convergence. All analyses were converged at least to the order of 10^{-6} for the second order accurate solution. Figure 19 indicates sample convergence characteristics of a solution. Moreover, Figure 20 and Figure 21 belong to the convergence of inlet Mach number and mass flow rate difference between inlet and exit of the domain respectively (NACA 65 906 - 1206 $K_{21}=50^\circ$ case).

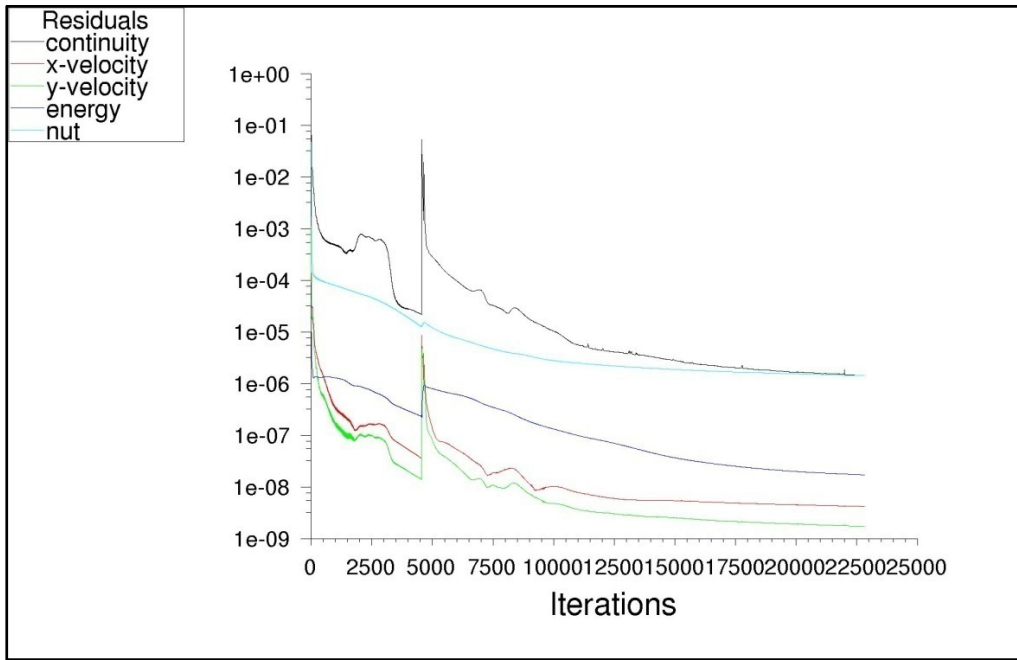


Figure 19 Residuals (NACA 65 906 - 1206 $K_{21}=50^\circ$ case)

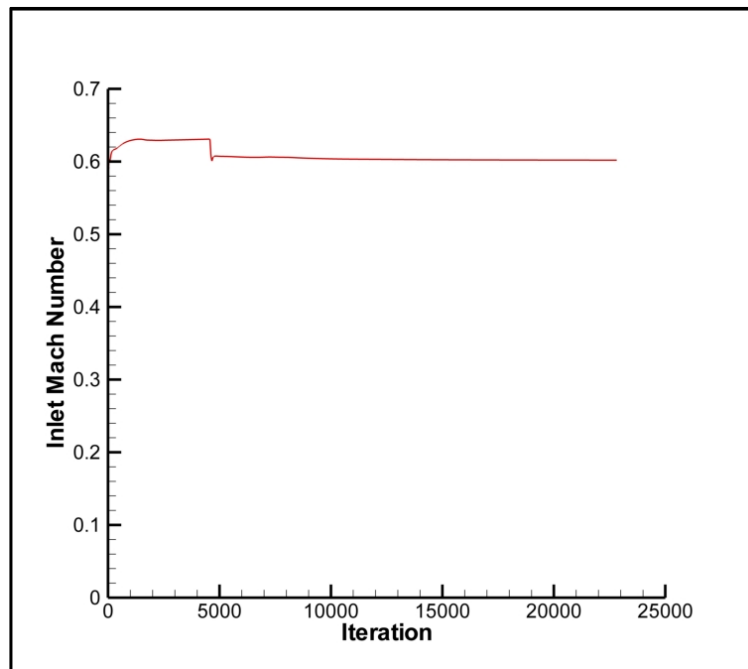


Figure 20 Convergence of Inlet Mach Number (NACA 65 906 - 1206 $K_{21}=50^\circ$ case)

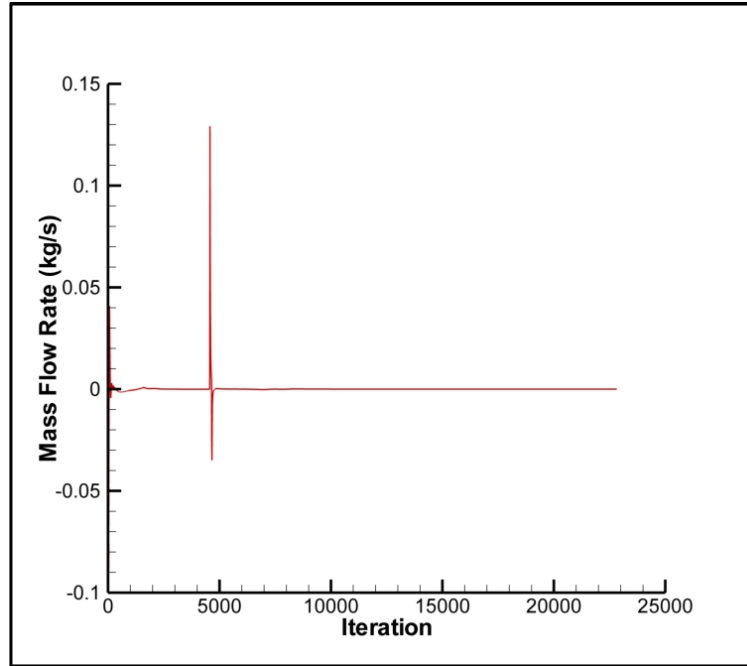


Figure 21 Convergence of Inlet-Outlet Mass Flow Difference (NACA 65 906 - 1206 $K_{21}=50^\circ$ case)

In Figure 19, Figure 20 and Figure 21 sharp peaks and bottoms present the change of boundary conditions. If desired inlet Mach number can't be reached by the first trial, most probably not, then back static pressure is changed to obtain the target Mach number at the inlet. Therefore, some sharp changes observed in the convergence graphs.

4.1.1 NACA 65 506-606

Starting airfoil pair was 506 – 606. Figure 22 shows geometries for different inlet blade metal angles. CFD analyses were performed for geometries which are listed in Table 8.

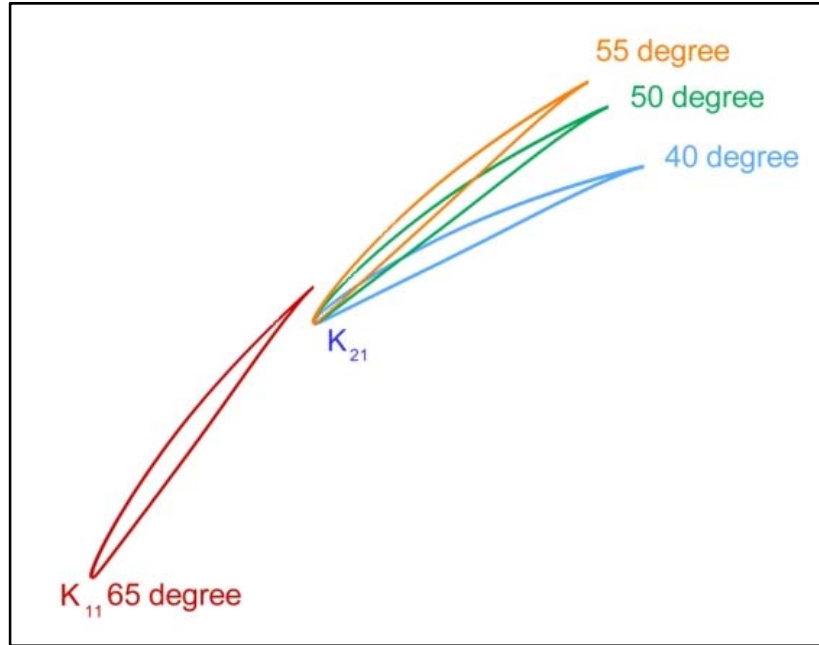


Figure 22 NACA 65 506-606 Airfoil Pair With Inlet Blade Metal Angles

Table 8 Geometry and Performance Values of 506-606 Pair

K ₁₁	K ₂₁	Φ _{overall}	D	ω _c	ω _p	Normalized Loading	
						FA	AA
65	55	39.70	0.450	0.026	0.016	0.61	0.39
65	50	44.70	0.523	0.028	0.020	0.59	0.41
65	40	54.70	0.600	0.056	0.050	0.57	0.43

It is seen from Table 8 that as K₂₁ decreasing, both D-factor and losses are increasing. Although K₂₁=40° case seems to have the highest D, ω_c and ω_p values this is not a practical case due to separation problem. Figure 23 indicates the full loss bucket of this case and obviously it is not showing an ordinary behavior. Such a useless configuration led to take a precaution for further analyses. From this analysis on the difference between airfoil inlet blade metal angles (K₁₁- K₂₁) was kept below 15° and systematically increased from 5° to 10° and 15°.

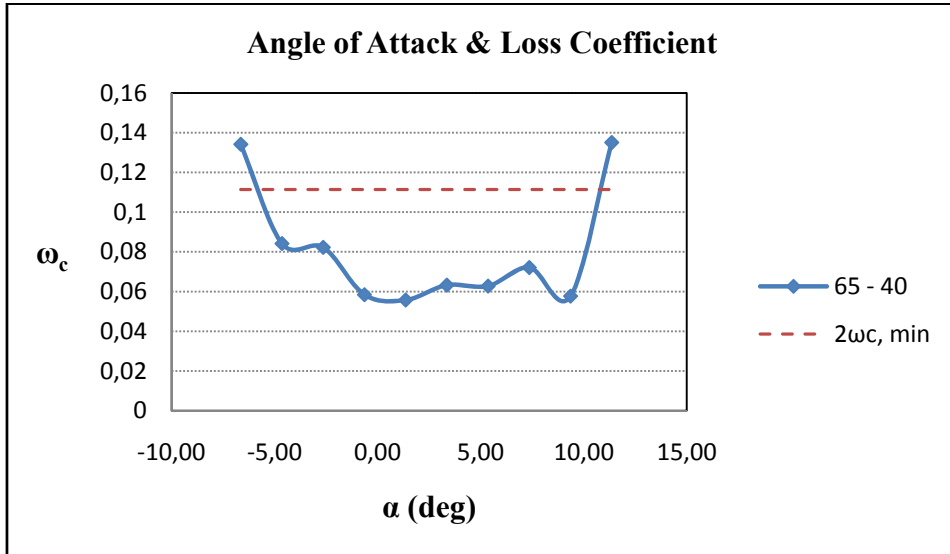


Figure 23 Loss Bucket of Separated Case ($K_{21}=40^\circ$)

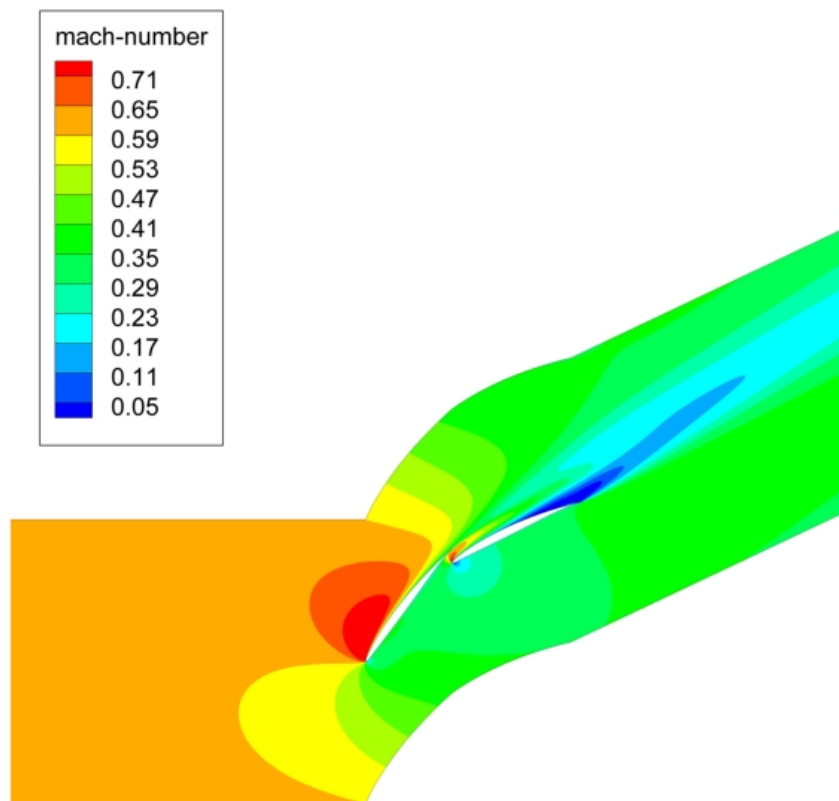


Figure 24 Mach Contours of Separated Case ($K_{21}=40^\circ$)

After elimination of separated tandem airfoil configuration, $K_{21}=50^\circ$ case has the highest diffusion and loss values as expected. Loading distribution did not change much between $K_{21}=50^\circ$ and 55° cases. However, loss parameter increased 25%, and D-factor increased 16%.

Figure 25 shows Mach distribution of $K_{21}=50^\circ$ case for NACA 65 506 - 606 tandem airfoil combination. As expected, the gap between forward and aft airfoil behaved like a nozzle and gave impetus to the flow passing through it.

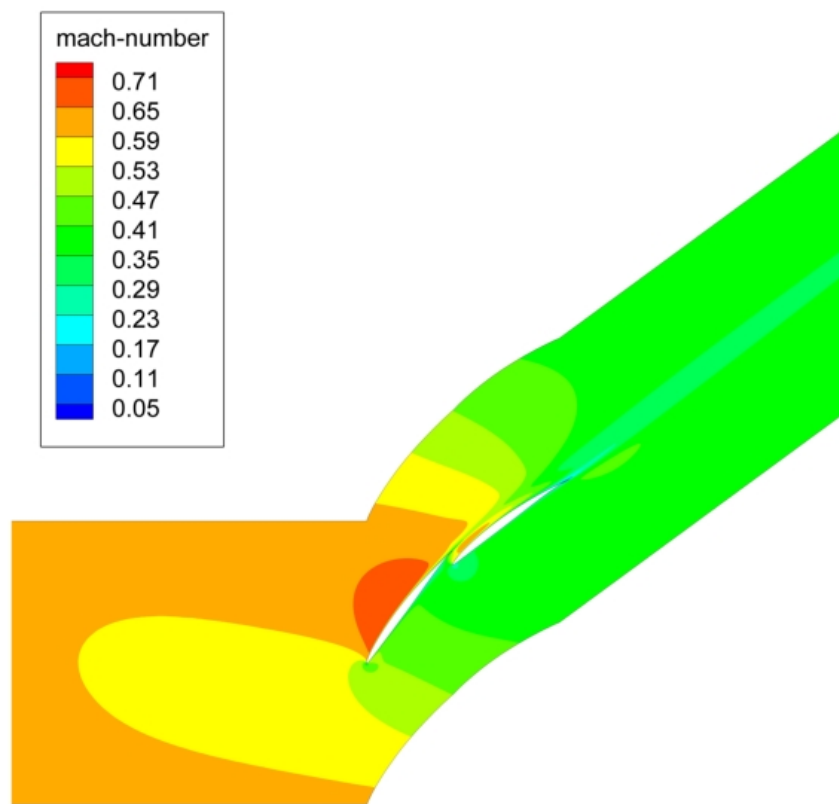


Figure 25 Mach Distribution of $K_{21}=50^\circ$ Case

4.1.2 NACA 65 506-906

In this part, three different NACA 65 506 - 906 tandem airfoil geometry was investigated. Figure 26 shows airfoil placements for all cases. Obtained results for design points are presented in Table 9.

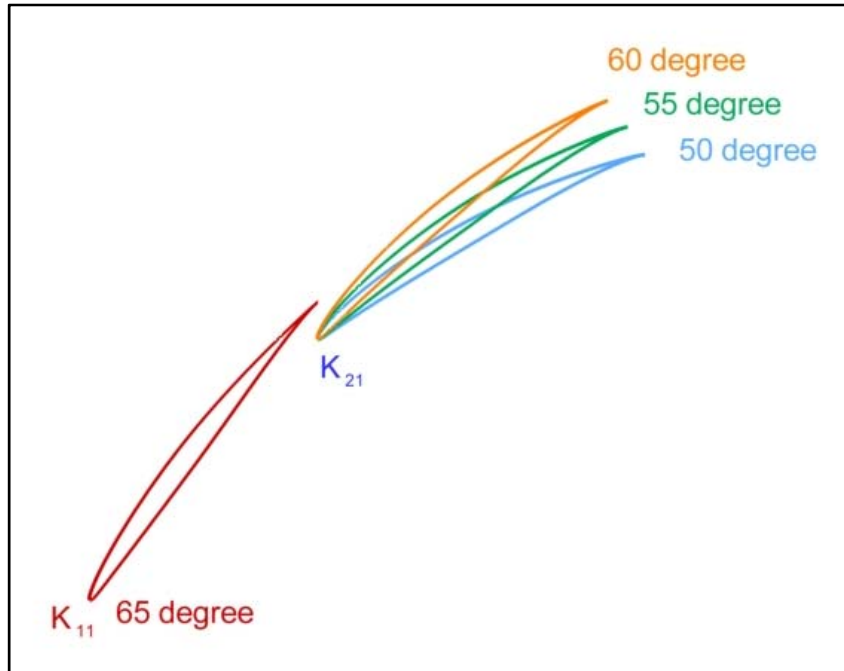


Figure 26 NACA 65 506 - 906 Airfoil Pair With Inlet Blade Metal Angles

Table 9 Geometry and Performance Values of 506-906 Pair

K ₁₁	K ₂₁	Φ _{overall}	D	ω _c	ω _p	Normalized Loading	
						FA	AA
65	60	48.37	0.507	0.026	0.018	0.58	0.42
65	55	53.37	0.575	0.028	0.023	0.57	0.43
65	50	58.37	0.563	0.030	0.024	0.49	0.51

Results indicate that highest diffusion belongs to $K_{21}=55^\circ$ case. However, highest loss values are seen at $K_{21}=50^\circ$. Expected trend for these analyses was increasing camber should lead to an increase in D-factor and loss values. Nonetheless, D-factor is first increasing with camber (Φ_{overall} 48.4° to 53.4°) then decreasing (Φ_{overall} 53.4° to 58.4°). Hence, if higher than 53° degree of camber is acquired for a design, second airfoil should be changed with a more cambered one rather than further decreasing K_{21} to obtain higher overall camber.

Moreover, it seems that increasing the overall camber has balanced the loading of forward and aft airfoils. This result contradicts with reference [1] where it was asserted that equal loading of airfoils would give the best results in terms of performance. Although lift distribution is nearly equalized for $K_{21}=50^\circ$ case, it showed the worst loss characteristics [1]. However, loading calculation method might be different in reference [1] then in this work. Assumption for the lift calculation was expressed at the beginning of this chapter and may result in such a contradiction.

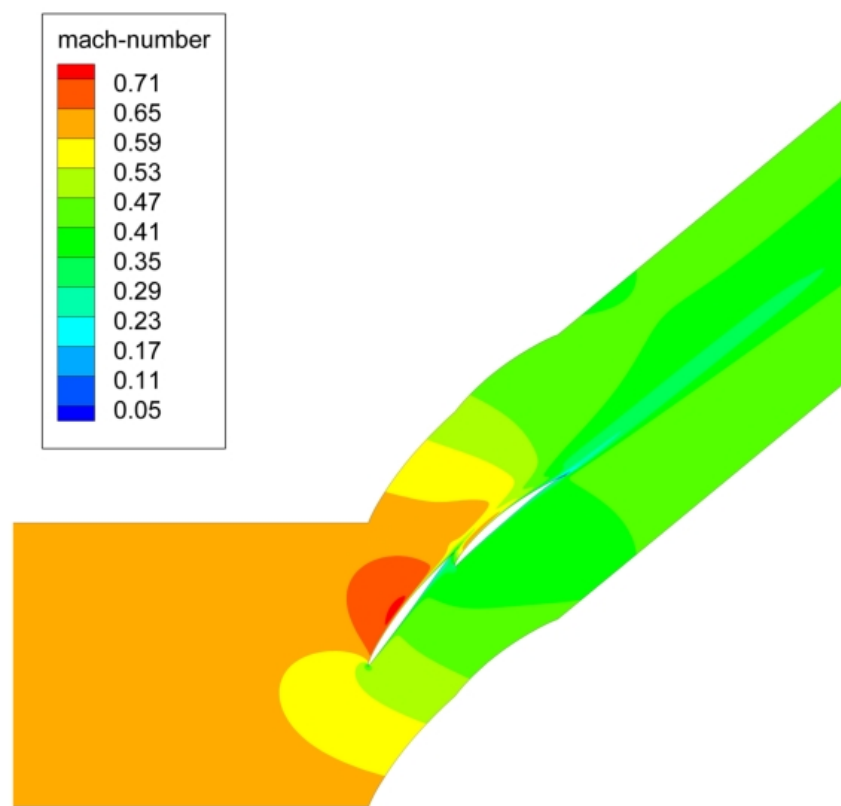


Figure 27 Mach Distribution of $K_{21}=60^\circ$ Case

Lastly, a 2-D single airfoil counterpart in terms of camber was built up and same performance analyses were performed for $K_{21}=60^\circ$ case. This was to see the superiority of a tandem airfoil on a single one in numbers. In Table 10 results are compared.

Table 10 Comparison of Single – Tandem Airfoil

Parameters	NACA 65 506 – 906	NACA 65 1006
Overall Camber	48.4°	47.7°
D-Factor	0.507	0.484
Loss Parameter	0.0183	0.0188
Loss Coefficient	0.0262	0.0283

Tandem airfoil seems to be 4.8% better in D-Factor, 2.7% and 7.4% lower respectively in loss parameter and loss coefficient.

Figure 28 represents the Mach contours of single airfoil case (NACA 65 1006).

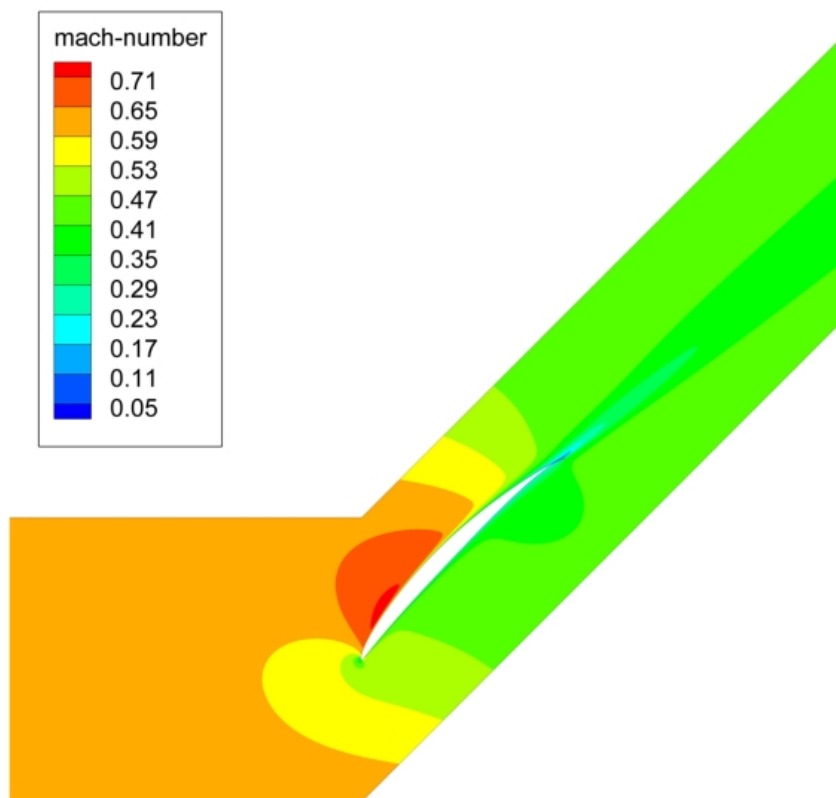


Figure 28 Mach Contours of Single Airfoil (NACA 65-1006)

4.1.3 NACA 65 506-1206

As similar as the previous airfoil combination, just the aft airfoil had been changed and became more cambered in this part. Airfoil pair NACA 65 506 - 1206 is illustrated in Figure 29 with two different inlet blade metal angle for the aft airfoil and CFD results are summarized in Table 11.

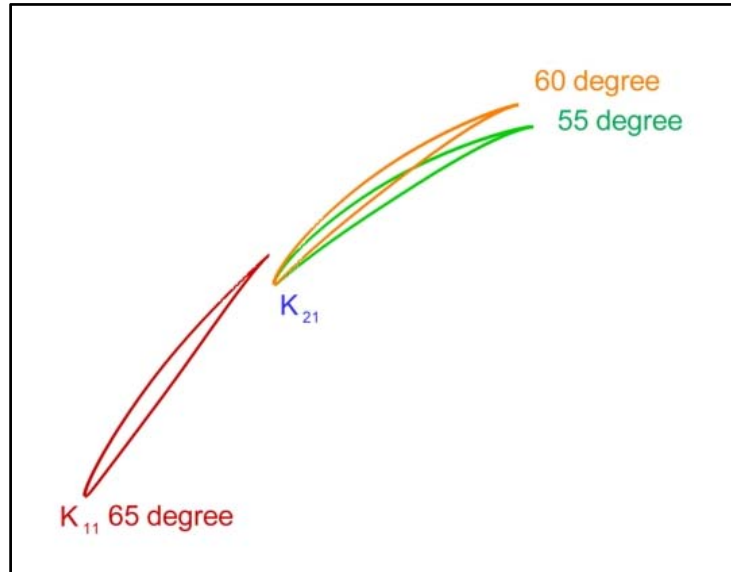


Figure 29 NACA 65 506-1206 Airfoil Pair With Inlet Blade Metal Angles

Table 11 Geometry and Performance Values of 506-1206 Pair

K ₁₁	K ₂₁	Φ _{overall}	D	ω _c	ω _p	Normalized Loading	
						FA	AA
65	60	60.87	0.485	0.025	0.019	0.51	0.49
65	55	65.87	0.534	0.027	0.022	0.51	0.49

It is observed in Table 11 that K₂₁=55° case has higher D-factor and higher losses which is not surprising. Both cases' loading distribution is interestingly the same (differs in third decimal) and they are very close to each other. Although this configuration has a higher overall camber, NACA 65 506-906

pair seems performed better in terms of diffusion and losses. Therefore, no further analysis planned for increased overall camber with these pair of airfoils.

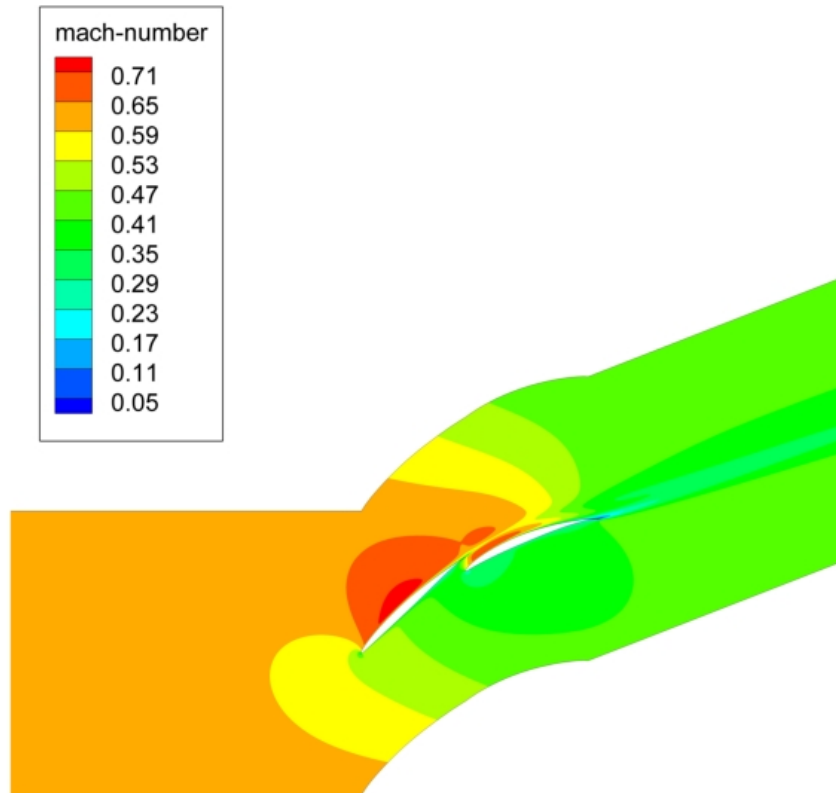


Figure 30 Mach Distribution of $K_{21}=55^\circ$ Case

4.1.4 NACA 65 906-1206

It is acquired from the former part that increasing camber of both airfoils may be useful for further increase in D-factor with tolerable loss values. Thus, NACA 906-1206 pair was investigated in this part. Camber levels were between 60° - 70° for this case which were the most cambered geometries in cascade analyses. Geometry of each case is shown in Figure 31 and results are listed in Table 12.

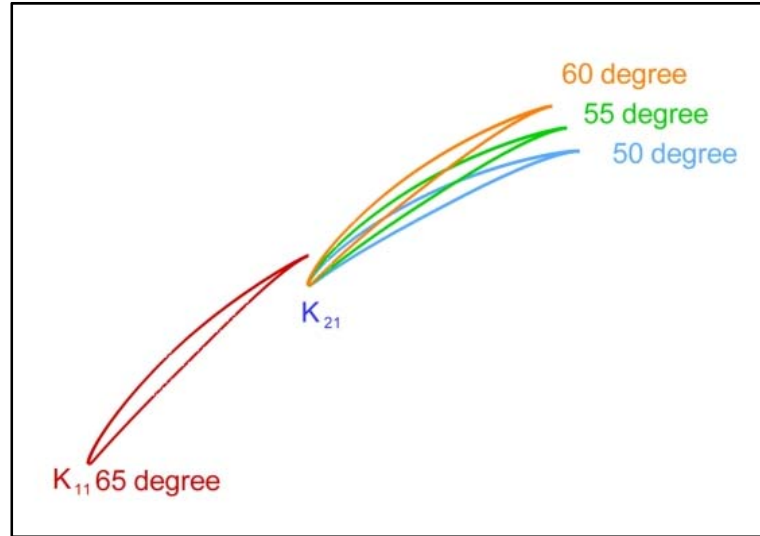


Figure 31 NACA 65 906 - 1206 Airfoil Pair With Inlet Blade Metal Angles

Table 12 Geometry and Performance Values of 906-1206 Pair

K ₁₁	K ₂₁	Φ _{overall}	D	ω _c	ω _p	Normalized Loading	
						FA	AA
65	60	60.87	0.432	0.034	0.023	0.72	0.28
65	55	65.87	0.468	0.028	0.020	0.62	0.38
65	50	70.87	0.531	0.027	0.022	0.60	0.40

Looking at results, consistency between overall camber and D-factor is seen first. Highest D-factor belongs to the K₂₁=50°. On the other hand highest losses obtained for K₂₁=60° which shows there is something unusual. This is due to the fact that forward airfoil having much camber than any other forward airfoil so that 5° difference in blade metal angles is probably not enough for a good flow path over these airfoil pair. Figure 32 illustrates Mach distribution for this case.

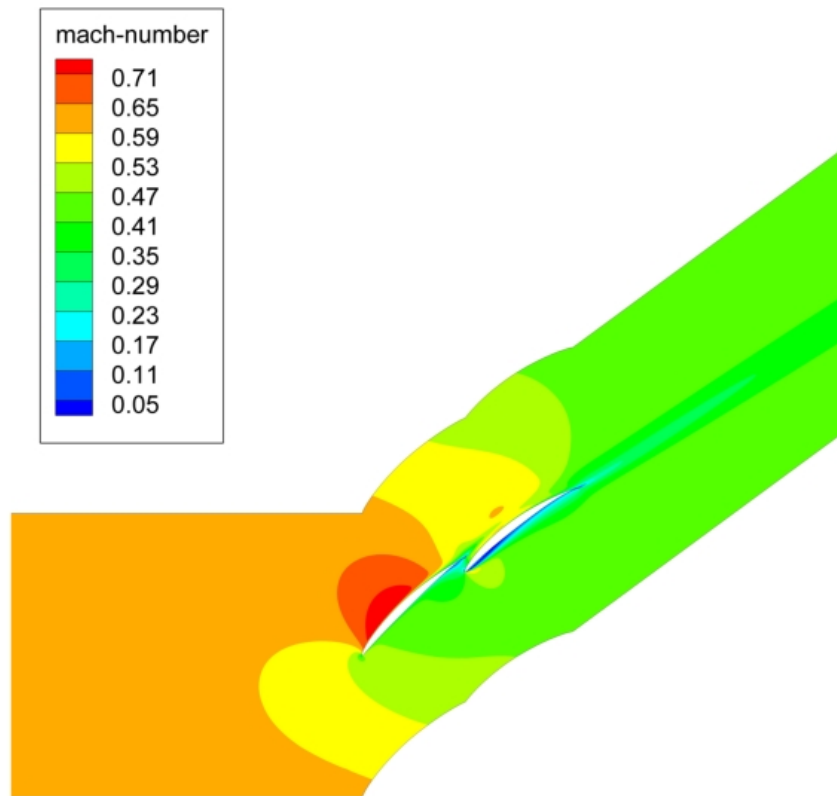


Figure 32 Mach Distribution of $K_{21}=60^\circ$ Pair

It is obviously seen that flow can't be expanded enough through the gap between two airfoils. Moreover, aft airfoil doesn't have a good inlet flow angle so that flow hits on the suction side and slowed down too much at the pressure side. Nonetheless, if inlet blade metal angle for the aft airfoil is decreased to 50° , then a good Mach contour is obtained around airfoils. Figure 33 indicates the Mach distribution of $K_{21}=50^\circ$ case.

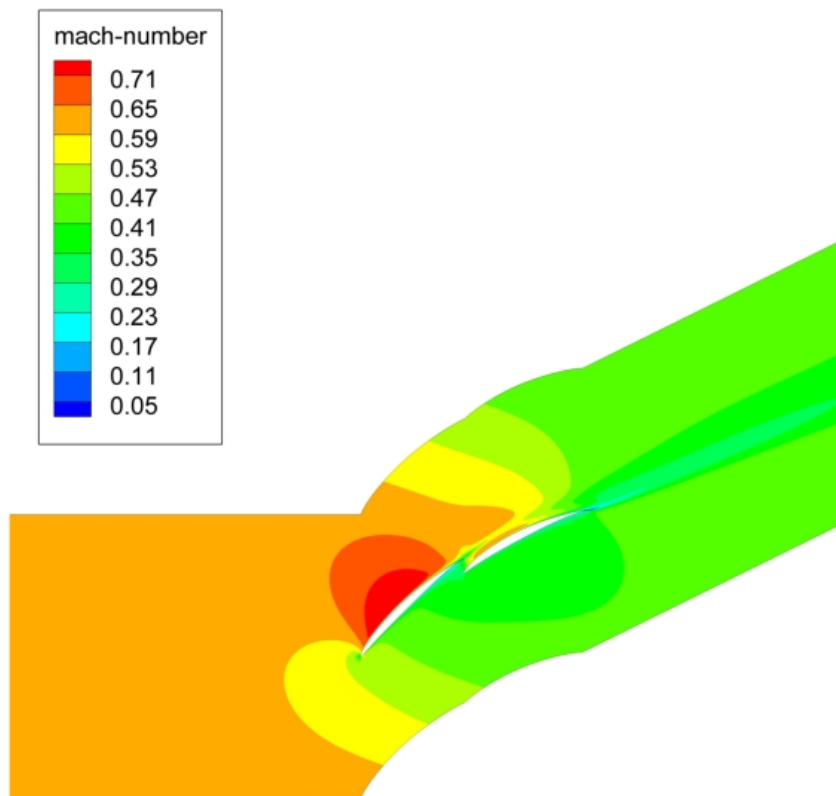


Figure 33 Mach Contours of $K_{21}=50^\circ$ Case

4.2 Generalization of 2-Dimensional Results

Four different airfoil pairs were investigated during the cascade study. K_{21} had been changed within a 15° range and performance values gathered. Figure 34 shows D-factor – loss relation and comparison with the single airfoil performance. Single airfoil performance values were taken from reference [1].

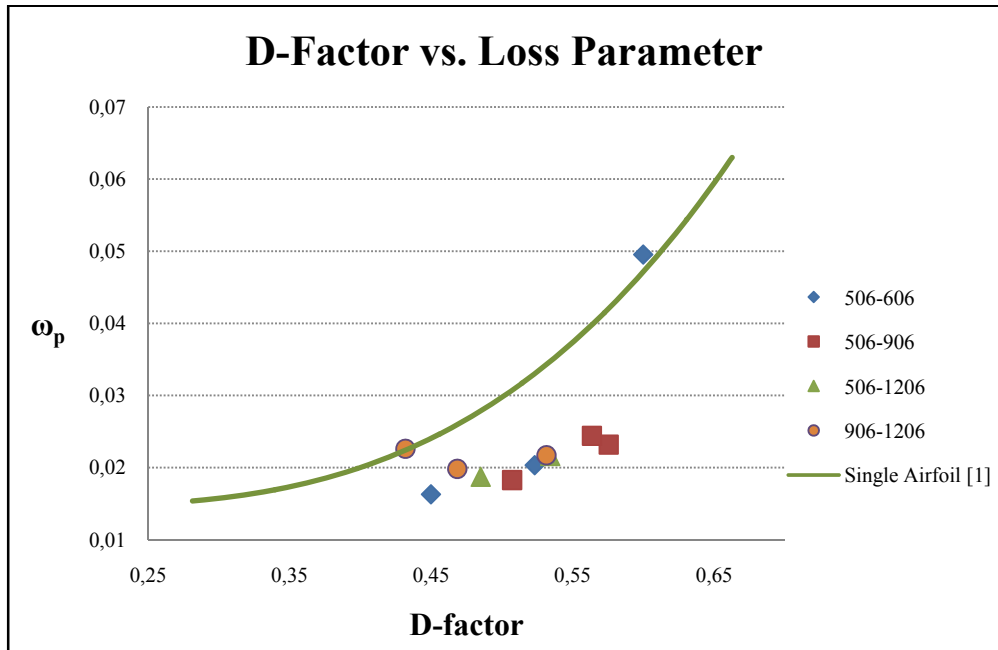


Figure 34 Scatter of Tandem Airfoil Performance Values

Figure 34 indicates that tandem airfoil application can achieve desired loading with lower loss values than a single airfoil. However, there are two points which are showing nearly the same performance with a single airfoil or even worse. This is due to corresponding tandem airfoil configurations have either separated flow or bad inlet flow angle for the aft airfoil. These results should lead somebody to understand that how tandem airfoil combination was built is very important.

Moreover, Figure 34 shows that D-factor range was 0.4-0.6. If one wants to go higher diffusion values may change the airfoil family and/or increase the solidity of cascade. This work was based on just one family of airfoils and a constant solidity of 1. Besides, for this study further increase in the overall camber may not be logical because a 70° overall camber was reached at the end.

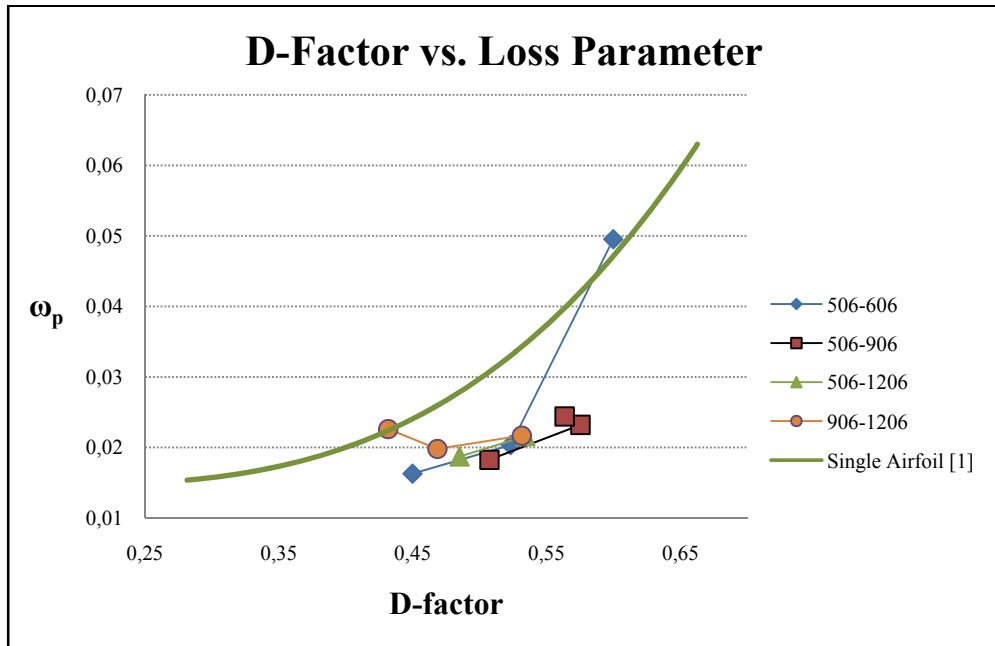


Figure 35 Loss-Loading Trends of Different Tandem Airfoil

Figure 35 illustrates the same things with Figure 34, just points were connected by lines to see tandem airfoil performance trend.

Figure 36 represents change of D-factor by overall camber. 506-606 pair $K_{21}=40^\circ$ case has the highest D-factor with a 54.7° of overall camber. However, it is useless because flow was separated easily (Look at Figure 23). Then it is practical to say that highest D-factor value was obtained from NACA 65 506-906 pair for $K_{21}=55^\circ$. However, somebody should look at the loss characteristics of those airfoil pairs before freezing the geometrical configuration of a tandem airfoil (Look at Figure 37).

In Figure 36 506-906 pair has a lower D-factor for 58° overall camber than 53° . On the other hand 58° has a higher loss parameter value which is indicated in Figure 37. This was due to the limitation of aft airfoil's inlet blade metal angle and explained before. Therefore, somebody should go and use airfoils having higher camber for the aft airfoil rather than changing K_{21} to obtain higher cambers. Another extraordinary result was seen for 906-1206 pair

having 60° and 65° cambered configurations. Between those two configurations, increasing camber increases D-factor but decreases loss parameter which was due to the unsuitable alignment of aft airfoil.

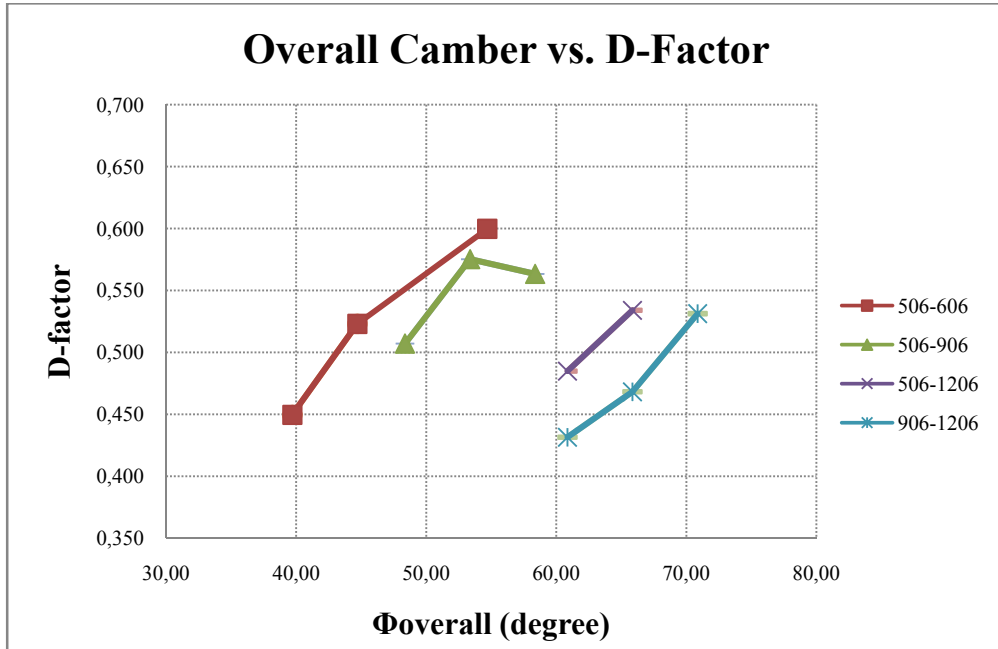


Figure 36 Change of D-factor by Overall Camber

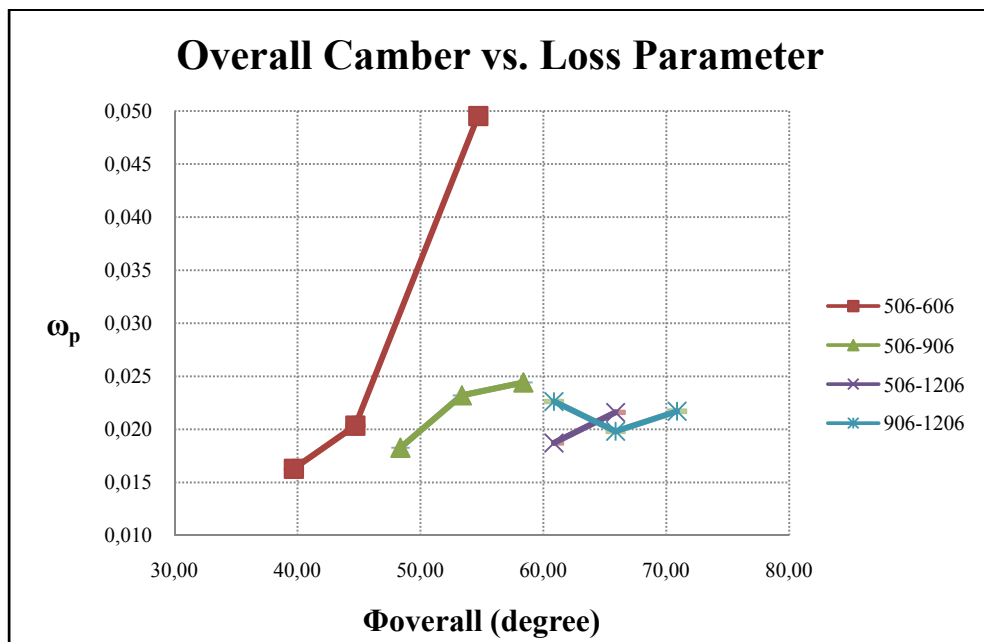


Figure 37 Change of Loss Parameter by Overall Camber

As expressed earlier, 906-1206 pair 61° cambered case does not work properly. It is clear in Figure 37, this case has higher loss than more cambered and more loaded tandem airfoil combinations which make it illogical to use.

At the end, it can be said that NACA 65 506-906 pair gave the best performance with a 53.4° overall camber. This case has the highest D-factor among useful tandem airfoil geometries and loss parameter value is rather good for such a diffusion factor. Moreover, Figure 34 and Figure 35 illustrate the difference between single and tandem airfoil configuration in terms of losses. The highest loss parameter difference between tandem and single airfoil at a certain D-factor was obtained for 506-906 pair 53.4° case ($K_{21}=55^\circ$). For such a configuration tandem airfoil nearly has the half of single airfoil loss for a D-factor of 0.58.

CHAPTER 5

CONCLUSION

4.3 Main Results

The main purpose of this thesis work was evaluating tandem airfoil performance in cascade flow. A number of 2-D CFD analyses were performed to observe loading and loss characteristics. Results were looking similar to the literature except the loading distribution between forward and aft airfoils. Moreover, considering Figure 34 one can say that tandem blade idea worth to work on.

Geometries for analyses were prepared such that second airfoil was always more cambered. This is because of the improved separation characteristics of tandem blades where flow can bare higher turning angles over second airfoil. However, this tolerance is up to a point. If the difference between inlet blade metal angles (K_{11} - K_{21}) increased too much, even for 15° trials, it was seen that tandem airfoil performance may drop drastically without separation occurring.

Comparison between a single airfoil and a tandem airfoil configuration both having same degree of turning angle showed that tandem configuration performs better. In numbers, tandem airfoil had 4.8% higher D-Factor value, 2.7% and 7.4% lower values in loss parameter and loss coefficient respectively.

4.4 Future work

A methodology based on commercial codes was developed during this study which makes repeated things easy to do. The in-house code was carrying out the very basics of design procedure and interacting analysis tools. In the future, adding some subprograms to this algorithm enlarges its capability and this program may be able to work on different type of airfoils, control a whole cascade CFD analysis automatically and draw 3-D geometries. In short, it may be doing axial compressor stage design by the help of other commercial programs. Therefore, this in-house code is a beginning for further studies.

Results showed that tandem blade performance is highly dependent on how overall camber is achieved. Even they are in the same airfoil family selection of airfoils and angular placements with respect to each other are crucial for obtaining best performance from tandem configuration. As a result, tandem blade idea becomes an optimization problem for obtaining desired overall camber. As a future study, optimization may be put on this thesis work to get better results. Moreover, some design rules may be obtained from optimization work or at least rule of thumbs which are to be used in tandem airfoil design.

REFERENCES

- [1]. McGlumphy, J., “Numerical Investigation of Subsonic Axial-Flow Tandem Airfoils for a Core Compressor Rotor”, Ph.D. Thesis, Virginia Polytechnic Institute and State University, 2008.
- [2]. Canon F., “Numerical Investigation of the Flow in Tandem Compressor Cascades”, Diploma Thesis, Vienna University of Technology Institute of Thermal Powerplants, 2004.
- [3]. Bammert, K., Staude., R., “Optimization for Rotor Blades of Tandem Design for Axial Flow Compressors”, *ASME Journal of Engineering for Power*, April 1980, pp. 369-375, 1980.
- [4]. Bammert, K., Beelte, H., “Investigations of An Axial Flow Compressor with Tandem Cascades”, *ASME Journal of Engineering Power*, October 1980, pp. 971-977, 1980.
- [5]. Nezym V.Y., Polupan, P.G., “A New Statistical-Based Correlation for The Compressor Tandem Cascade Parameters Effects on The Loss Coefficient”, ASME Paper GT2007-27245, 2007.
- [6]. Leiblein, S., *Aerodynamic Design of Axial-Flow Compressors*, Chapter VI, NASA SP -36 Report, 1965.
- [7]. Wennerstrom, A.J., “Highly Loaded Axial Flow Compressors: History and Current Developments”, *Journal of Turbomachinery*, October 1990, Vol. 112, pp. 567-578, 1990.
- [8]. Wennerstrom, A.J., “Low Aspect Ratio Axial Flow Compressors: Why and What It Means”, *Journal of Turbomachinery*, October 1989, Vol. 111, pp. 357-365, 1989.
- [9]. Ball, C.L., “Advanced Technolgy's Impact on Compressor Design and Development: A Perspective”, SAE International Paper 892213, 1989.

- [10]. Jonathan McGlumphy, Wing-Fai Ng, Steven R. Wellborn, Severin Kempf, “Numerical Investigation of Tandem Airfoils for Subsonic Axial-Flow Compressor Blades”, *Journal of Turbomachinery*, Vol. 131, pp. 021018 1-8, April 2009.
- [11]. McGlumphy, J., Ng, W., Wellborn, S.R., Kempf, S., “ 3D Numerical Investigation of Tandem Airfoils for A Core Compressor Rotor”, *Journal of Turbomachinery*, Vol. 132, pp. 031009 1-9, July 2010.
- [12]. Aungier, R.H., *Axial-Flow Compressors: A Strategy for Aerodynamic Design and Analysis*, ASME Press, New York, 2003.
- [13]. Cumpsty, N.A., *Compressor Aerodynamics*, Harlow, Essex, England : Longman Scientific & Technical ; J. Wiley, New York, 1989.
- [14]. Mattingly, J.D., *Elements of Gas Turbine Propulsion*, AIAA, Inc., Reston, Virginia, 2006.
- [15]. Hill, P.G., Peterson, C.R., *Mechanics and Thermodynamics of Propulsion*, Addison-Wesley, Mass., 2010.
- [16]. Abbott, H., Doenhoff, A.E., *Theory of wing sections*, Dover Publications, Inc., New York, 1959.
- [17]. Ladson, C.L., Brooks, C.W., Hill, A.S., Sproles, D.W., “Computer Program To Obtain Ordinates for NACA Airfoils”, *NASA Technical Memorandum 4741*, December 1996.
- [18]. *Fluent v6.3 User’s Guide*, 2006.
- [19]. Najero, A.A., “3D Design and Simulations of NASA Rotor 67”, M.Sc. Thesis, University West, 2008.
- [20]. *Numeca Fine Turbo v8.c Tutorial Guide*, October 2007.

- [21]. Ling, J., Wong, K.C., Armfield, S., “Numerical Investigation of A Small Gas Turbine Compressor”, Australian Fluid Mechanics Conference, 2-7 December 2007.
- [22]. Belamri, T., Galpin, P., Braune, A., Cornelius, C., “CFD Analysis of A 15 Stage Axial Compressor Part I: Mmethods”, ASME Paper 2005-68261, 2005.
- [23]. Wallis, C.V, Moussa, Z.M., Srivastava B.N., “A Stage Calculation in A Centrifugal Compressor”, International Council of The Aeronautical Sciences (ICAS), 2002.
- [24]. *TecPlot 360 User Guide*, 2006.
- [25]. Wikipedia, Flap (Aircraft), [http://en.wikipedia.org/wiki/File:Airfoil_lift_improvement_devices_\(flaps\).png](http://en.wikipedia.org/wiki/File:Airfoil_lift_improvement_devices_(flaps).png) (Last accessed date: September 12th, 2012).
- [26]. Chima, R.V., “Calculation of Tip Clearance Effects in A Transonic Compressor Rotor”, NASA Technical Memorandum 107216, 1998.
- [27]. Zante, D.E., Strazisar, A.J., Wood, J.R., Hathaway, M.D., Okiishi, T.H., “Recommendations for Achieving Accurate Numerical Simulation of Tip Clearance Flows in Transonic Compressor Rotors”, NASA/TM-2000-210347, September 2000.
- [28]. NASA, Wall y^+ , <http://geolab.larc.nasa.gov/APPS/YPlus/> (Last accessed date: September 22nd, 2012).

APPENDIX A

PRESSURE INLET vs. PRESSURE FAR FIELD BOUNDARY CONDITOINS

While comparing these two upstream boundary conditions, same flow domain geometries were used for both analyses. Exit boundary conditions were exactly the same as well. This flow domain was created using a NACA 65 506 – 906 pair having a percent pitch of 0.90, a solidity of 1 and blade metal angles were $K_{11}=65^\circ$ and $K_{21}=55^\circ$. Obtained performance results were tabulated in Table 13.

Table 13 Comparison of Performance Values

	Pressure Inlet	Pressure Far Field
D	0.5690	0.5665
ω_p	0.0276	0.0274
ω_c	0.0344	0.0342

It is clearly seen that D, ω_p and ω_c values does differ less than 1%.

Another comparison was made for the loading of airfoils. As seen in Table 14 they also do differ less than 1%.

Table 14 Comparison of Loading

Airfoil	Normalized Lift	
	Pressure Inlet	Pressure Far Field
FA	0.503	0.501
AA	0.497	0.499

Lastly Mach contours for these two CFD solution were given in Figure 38 and Figure 39. Mach number distributions are looking so similar that around airfoils and at the gap between airfoils nearly the same.

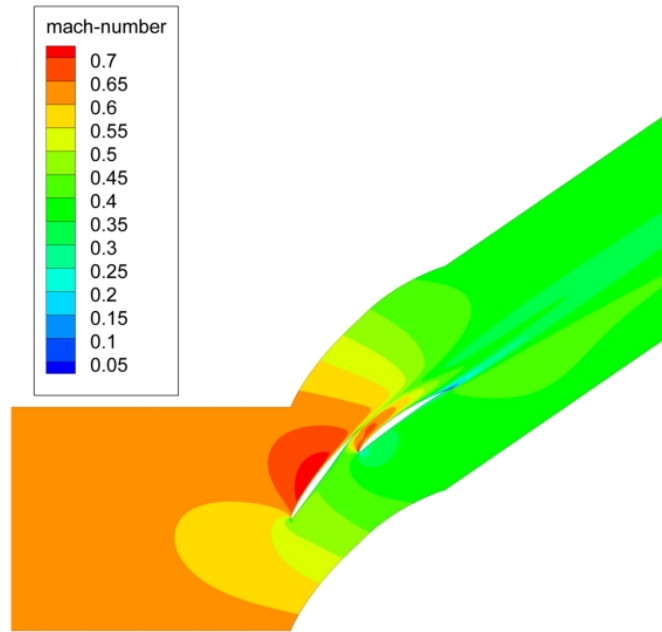


Figure 38 Mach Contours of Pressure Inlet Case

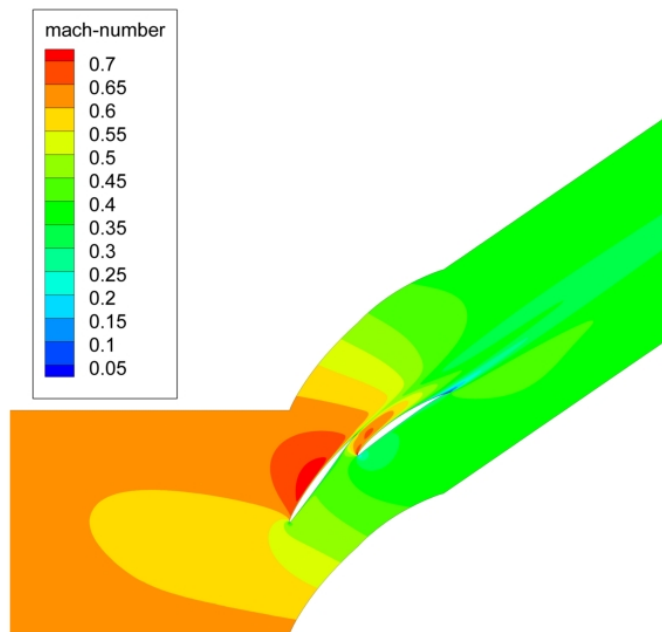


Figure 39 Mach Contours of Pressure Far Field Case